THESIS FOR THE DEGREE OF DOCTOR OF PHILOSOPHY (PHD)

Temporomandibular Joint Involvement in Mice with Proteoglycan Induced Arthritis and the Role of TSG-6 in Proteoglycan Induced Arthritis

by Sheida Ghassemi Nejad, AAS, DMD

UNIVERSITY OF DEBRECEN
DOCTORAL SCHOOL OF CLINICAL MEDICINE

DEBRECEN, 2019

THESIS FOR THE DEGREE OF DOCTOR OF PHILOSOPHY (PhD)

Temporomandibular Joint Involvement in Mice with Proteoglycan Induced Arthritis and the Role of TSG-6 in Proteoglycan Induced Arthritis

Written by: Sheida Ghassemi Nejad AAS, DMD
Supervisor: Prof. Zoltán Szekanecz MD, DSc

UNIVERSITY OF DEBRECEN
DOCTORAL SCHOOL OF CLINICAL MEDICINE

DEBRECEN, 2019

Table of Contents

Keywords and List of Abbreviations

Keywords

Aggrecan
Animal model
Antigen
Cartilage
Cytokine
Extracellular Matrix
Heparin
Hyaluronate
Inflammation
Mast Cell
Mouse
Osteoarthritis
Proteoglycan-induced arthritis
Rheumatoid arthritis
Temporomandibular joint
TSG-6

Abbreviations

Ab: antibody
Ag: antigen
Apc: allophycocyanin
APC: antigen-presenting cell
autoAb: autoantibody
autoAg: autoantigen
CI: confidence interval
CIA: collagen-induced arthritis
CII: type II collagen
DC: dendritic cell
DDA: dimethyl dioctadecyl-ammonium bromide
EGFP-LysM KI: enhanced green fluorescent protein-lysozyme M knock-in
FL-HA: fluorescein-conjugated HA

GAG: glycosaminoglycan
GC: germinal center
HA: hyaluronan
HC: heavy chain
IFN-γ: Interferon gamma
IL: Interleukin
IP: immunoprecipitation
IαI: inter-α-inhibitor
JDLN: joint-draining lymph node
LN: lymph node
mAb: monoclonal antibody
MHC: major histocompatibility complex
mMCP-6 and -7: murine mast cell protease-6 and -7, respectively
OVA: ovalbumin (from chicken egg white)
PBS: phosphate-buffered saline
PG: proteoglycan (cartilage aggrecan)
PGIA: proteoglycan-induced arthritis
RA: rheumatoid arthritis
rmMCP-6 and -7: recombinant mouse MCP-6 and -7, respectively
rmTSG-6: recombinant mouse TSG-6
SCID: severe combined immunodeficient
TCR: T cell receptor
Teff: effector T cell
Tfh: follicular T helper cell
Tg: transgenic
Th: T helper
TMB: tetramethylbenzidine substrate
TMD: temporomandibular joint disorder
TMJ: temporomandibular joint
TNF-α: tumor necrosis factor alpha
TPM: two-photon microscopy
Treg: regulatory T cell
WT: wild type

Introduction

The pathology of temporomandibular joint arthritis

The temporomandubular joint is a ginglymoarthrodial (hinge and gliding) joint where the ball is formed by the mandibular condyle whilst the socket is provided by the glenoid fossa on the temporal bone. The joint is separated into two compartments – an upper and a lower – by a fibrocartilaginous disc. The anatomical structure of the joint allows a wide range of movement and the ability to absorb shock during mastication. It is one of the most frequently used joint which makes it susceptible to overuse related disorders. (1).

TMJ syndrome or temporomandibular joint disorder (TMD) is an embracing clinical term containing muscle and articular disorders which therefore is multifactorial in origin. Bruxism (teeth grinding), impacts to the jaw, clenching (jaw tightening, trauma, ankylosis, arthritis, tumors and developmental anomalies are all known to be the cause of it (2). Symptoms of TMD can be pain around the head, face and neck region and it can be associated with certain types of headaches. Locking and reduced range of movement can also be associated with TMJ problems. Some patients also complain about jaw clicking, weak bite and also earache (otalgia) due to its anatomical proximity (3-6). Meniscus displacement, such as internal derangement disorder, or the development of OA-like degenerative changes of articular cartilage covering the mandibular condyle are among the most common cause of TMD [reviewed in (7, 8)].

One of the most common cause for TMJ pain is arthritis. Degenerative changes in the articular cartilage, meniscus displacement and rheumatoid arthritis can are all known to cause arthritis in this joint.

Osteoarthritis (OA) is a degenerative joint disease. It is the most common joint disease characterized by progressive softening and disintegration of the articular cartilage.

Development of OA is also multifactorial, different types of collagens, matrix metalloproteinases, SLRPs, cytokines and lifestyle choices all contribute to its early development (9). As a result of hereditary predisposition, developmental anomalies, various metabolic causes, mechanical overuse or just age related degenerative changes, damage to the cartilage leads to degradation of the subchondral bone and ultimately the destruction of the joint (10).

Rheumatoid arthritis (RA) is an autoimmune disease with a 0.5-1% prevalence in the human population. It is characterized by inflammation in the synovial joints including the TMJ. TMJ involvement is more common in the younger age groups. The disease leads to cartilage damage, bony erosions which result in deformities in the joints and ultimately complete loss of joint function. As a result, it can be very debilitating to patients (11, 12).

The prevalence of TMJ involvement in RA is thought to be 4 to 86% depending on the diagnostic methods and criteria used for patient selection (13, 14). Histopathological changes of the TMJ have not been thoroughly investigated. Some studies described the complete substitution of cartilage by fibrous tissue in later stages of RA (15). Arthroscopical investigation of the TMJ revealed both degenerative and inflammatory changes with fibrosis in both OA and RA (16). Based on available evidence it is no clear whether histopathological changes in the TMJ in patients in RA resembles inflammatory or degenerative changes this is in part due to the limited availability of human inflamed histological TMJ specimens.
In order to investigate the problem, multiple animal models of inflammatory TMJ conditions have been developed (9). Most of these models are centered around direct injection of antigen or adjuvant into the TMJ (17, 18).

PGIA is a murine model of RA that has multiple common characteristics with human RA including the clinical picture, radiological changes, serum cytokines, autoantibodies (RF) and anti-citrullinated protein antibodies. Although the peripheral joint and spine affected by PGIA have been thoroughly investigated, the also synovial TMJ has not yet been examined. For this reason we used BALB/c mice with PGIA to investigate the involvement of TMJ in the early and late phases of the disease (9) (19) (20).

Features of TSG-6

TSG-6 has been shown to function as an anti-inflammatory and chrondroprotective protein in response to growth factors (21) and pro-inflammatory mediators in many animal arthritis and inflammatory models like recombinant murine TSG-6 (rmTSG-6) model. It has also been detected in the synovial fluids and tissues of patients with RA in the affected joints (22, 23). It is a hyaluronan (HA) –binding protein (24) secreted by many cells from the tumor necrosis factor α-stimulated gene-6 (TNFAIP6 or TNFIP6).

TSG-6 consists of a "link" module and a "CUB" (complement C1s/C1r-, uEGF-, BMP-1-like) domain. The positively charged link module binds various glycosaminoglycans (GAGs), including HA, chondroitin sulfate, heparin, and heparan sulfate. The CUB domain of TSG-6 is similar to the CUB module found in several developmentally regulated proteins (25) that are thought to be involved in protein-protein interactions (26, 27). However, to date, only fibronectin has been shown to bind to the CUB domain of TSG-6 (28). Its expression is triggered by proinflammatory cytokines and LPS (22, 29, 30), whilst it is inhibited by direct or indirect suppression by IL-4 or IL-10 via inhibition of LPS/Toll-like receptor induced cell activation (30).

Reduced leukocyte influx into the arthritis joints have been observed in mice treated with TSG-6 (31, 32). These findings are consistent with other in-vitro studies which demonstrated inhibition of CD44-mediated adhesion of soluble HA TSG-6 complex treated leucocytes to immobilized HA (31-33). TSG-6 deficient mice on the other hand exhibited increased leukocyte extravasation into the joints (34). The reason for this is that TSG-6 modulates HA binding to its surface HA receptor CD44 (35). CD44 mediated adhesion of leukocytes on HA-covered surfaces of inflamed vascular endothelium is required for the emigration of leucocytes from the bloodstream into inflamed tissue (36) therefore inhibition of this step by the HA-TSG-6 complex could have a negative impact on the extravasation of inflammatory cells. These observations suggest that through multiple pathways, TSG-6 has an important role in the resolution of inflammation.

Aims of the studies

In the studies included in the present thesis I have tried to find the answers for the following questions:

Study 1:

- Are there pathologic changes in the TMJ in mice with PGIA?
- If there are, do these changes resemble RA or OA?

Study 2:

- What is the function of TSG-6 in mice with PGIA?
- Is there a way to find a sensitive detection method to measure the concentrations of TSG-6 from BALB/c mice with PGIA?
- Do TSG-6 levels correlate with the severity of arthritis in mice with PGIA?
- Do TSG-6 levels correlate with immune responses?
- Is TSG-6 expressed in any tissues or cells during the development of PGIA?

Materials and methods

Study 1

Antigen, animals, immunization and assessment of peripheral arthritis

The collection of human OA cartilage from consenting patients undergoing total knee joint replacements was approved by the Institutional Review Board of Rush University Medical Center (Chicago, IL). PG (aggrecan) was extracted from OA cartilage and purified by gradient centrifugation, deglycosylated, characterized, and tested for arthritis induction as described (19, 37). Female BALB/c mice (12–16 weeks old) were purchased from Charles River Laboratories (Kingston Colony).

Animals were immunized according to the standard procedure for induction of PGIA, intraperitoneal injection was given with an emulsion of PG (100 μg of protein in 100 μl phosphate-buffered saline, PBS) and 2 mg dimethyl dioctadecyl-ammonium bromide (DDA) adjuvant (Sigma-Aldrich, St. Louis, MO) on days 0, 21, and 42 (37). Control mice were injected with an emulsion of PBS and DDA (without antigen) under the same schedule. All animal procedures were conducted under a protocol approved by the Institutional Animal Care and Use Committee of Rush University Medical Center.

Immunized mice were examined 2–3 times a week for clinical symptoms of arthritis, and after the second immunization we were able to record abnormalities due to arthritic changes of the joints. The time of onset and incidence of arthritis were recorded, and disease severity was scored in a blinded manner by two different investigators, based upon swelling and redness of each paw on a scale ranging from 0 to 4, yielding a potential maximum severity score of 16 for each animal (20, 38).

Arthritic mice were divided to an acute and a chronic group, The acute group (N=10) was sacrificed during the clinically determined acute phase of PGIA (see Fig. 1A, dotted-line arrow), i.e., 6–7 days after the onset of arthritis, when swelling and redness were steadily increasing in the distal joints of the limbs.

The chronic group (N=12) was sacrificed during the chronic phase of the disease (Fig. 1A, dashed-line arrow), i.e., approximately two weeks after the onset of arthritis (day 60 after the first PG/DDA injection), when swelling was still present, but hardening of the periarticular soft tissue, joint deformities and ankylosis dominated the clinical picture (10-26). PBS/DDA-injected (non-arthritic) control mice (N=8) were sacrificed with the chronic group on day 60.

Figure 1.

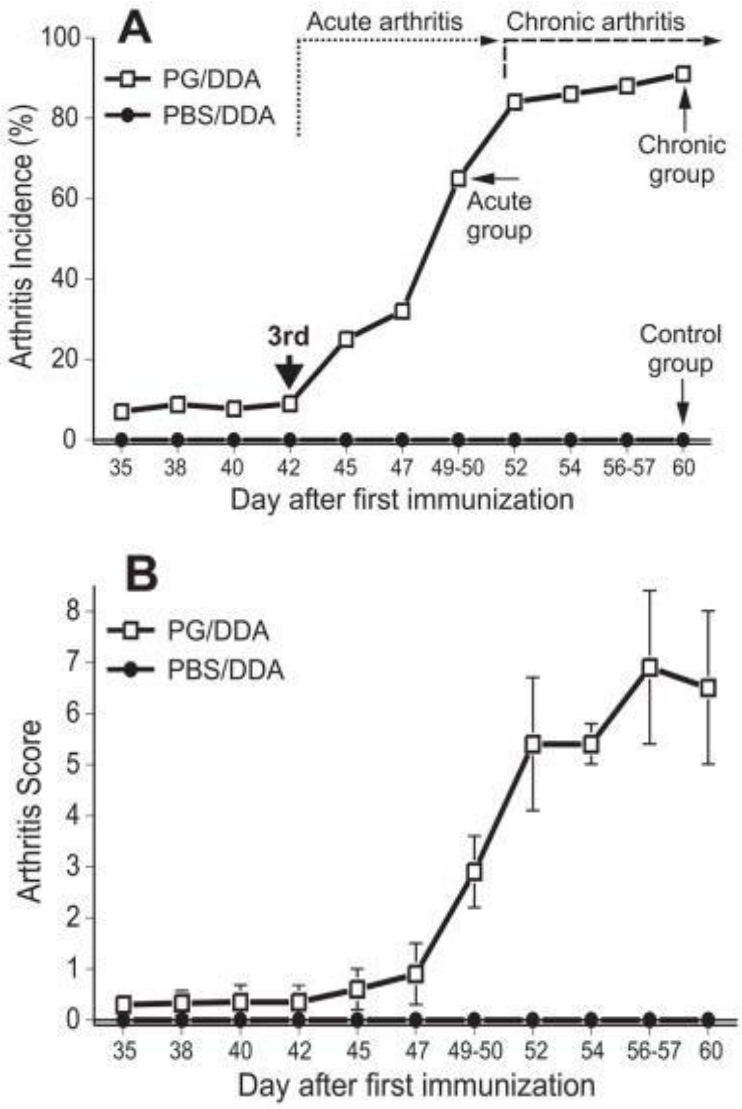

Figure 1. Incidence and severity of proteoglycan-induced arthritis (PGIA) in BALB/c mice used in this study. (**A**) Arthritis incidence is shown as the % of arthritic animals among all cartilage PG-immunized (PG/DDA-injected, N = 22) or adjuvant (PBS/DDA)-injected (N = 8) mice. Thick solid arrow points to the time of the 3rd PG/DDA or PBS/DDA injection. The approximate time frames of clinically determined acute and chronic phases of arthritis are indicated by dotted-line and dashed-line arrows, respectively. Thin solid arrows depict the time points at which groups of mice with acute (N = 10), and chronic (N = 12) arthritis, and non-arthritic control mice (N = 8) were sacrificed. (**B**) Disease severity in the same groups is expressed as a cumulative inflammation score. The data shown are the means (incidence) or the means ± 95% confidence levels (CI 95%) of disease severity scores.

Measurements of cytokines in serum samples

Blood was collected from control (PBS/DDA-injected) and arthritic mice at different time points of immunization, before and after the onset of arthritis (27-28-29-30). Concentrations of pro-inflammatory serum cytokines, including interleukin (IL)-1β, TNF-α, IL-6, and IL-17, were measured using capture enzyme-linked immunosorbent assays (ELISA) according to the manufacturers' instructions (BD Biosciences, San Diego, CA, or R&D Systems, Minneapolis, MN). Results were expressed as picograms (pg) of cytokine per ml serum.

Histology, histochemistry and immunohistochemistry

Dissection of hind limbs and heads were done from euthanized mice on day 49 or 50 (for mice with acute arthritis of peripheral joints) and from mice with chronic arthritis and control groups on day 60. Heads were cut in half in the sagittal direction, heads and paws were fixed in 10% neutral buffered formalin (Protocol Formalin, Fisher Scientific, Kalamazoo, MI). Limbs and heads were acid-decalcified and embedded in paraffin. The heads were carefully oriented in the paraffin blocks so that the sectioning blade could run parallel to the posterior mandible and the mandibular head. In order to evaluate structural integrity, staining of the deparaffinized sagittal serial sections (6–8 μm thick) of paws and TMJs were done with hematoxylin and eosin (Sigma), or with safranin O and fast green (Acros Organics, NJ) and assessed cartilage PG aggrecan loss (39) using standard histochemical methods described earlier (31). Sections from all experimental groups were stained simultaneously.

For immunohistochemistry (IHC), deparaffinized sections were rehydrated in 50 mMTris-acetate buffer (pH 7.4). The sections were digested with 0.5 units/ml chondroitinase ABC (Seikagaku Corp., Japan) dissolved in 50 mM Tris-acetate buffer for 60 min, to unmask the protein epitopes in cartilage (31).

Non-specific protein binding sites were blocked with 10% normal goat serum in PBS and then stained with rabbit antibodies specific to cartilage PG (aggrecan) neoepitopes. These antibodies were raised against the neoepitopes -VDIPEN^{341} and -NVTEGE^{373} (NITEGE in human) as described (31). Neoepitope -VIDIPEN is generated mostly by stromelysin (matrix metalloproteinase [MMP]-3) by cleaving the interglobular domain (IGD) of the core protein of cartilage PG aggrecan. NITEGE/NVTEGE is another cleavage product of the IGD by aggrecanase-1 (also known as a disintegrin and metalloproteinase with thrombospondin type 1 motif-4, ADAMTS-4), or aggrecanase-2 (ADAMTS-5) (40, 41).

Neoepitopes which are bound to hyaluronan *via* the G1 domain will be available for the respective antibodies after cleavage of the IGD of the aggrecan by these enzymes (31, 40).

The core protein released by the enzymes (the rest of the PG molecule), with negatively charged glycosaminoglycan (GAG) side chains, and diffuses out of the cartilage. As a result, the negatively charged GAGs, stained red with safranin O, are lost (39).

Rabbit antibodies were used at a 1:40 dilution, and the binding of the primary antibodies was detected with peroxidase-conjugated goat anti-rabbit IgG (Invitrogen, Carlsbad, CA). Digestion with chondroitinase ABC was sufficient for these antibodies to access the epitopes in the paraffin sections, and no antigen retrieval was necessary. Peroxidase reactions were developed with diaminobenzidine (DAB) chromogen and H_2O_2 substrate (Vector Laboratories, Burlingame, CA) as described (31).

All slides were exposed to DAB for the same length of time, and the specificity of immunostaining was ensured by replacement of the first antibodies with normal rabbit serum in one set of slides. All tissue sections were viewed under a Nikon Microphot-FXA (Nikon, Melville, NY) bright-field microscope. TIF images (in 24-bit color RGB mode) were generated using MetaView image acquisition software (Molecular Devices, Sunnyvale, CA).

Morphometric analysis of safranin O and immunohistochemical staining

Morphometric analyses were performed by a blinded investigator on the densities of Safranin O staining and immunohistochemistry (IHC; DAB staining), for quantitative image analysis using a modified version of a previously published Adobe Photoshop-based protocol (42). In brief, TIF images of tissue sections were opened in Adobe Photoshop (version 6, Adobe Systems, San Jose, CA), and 3 rectangular areas (corresponding to full-thickness cartilage in the middle and 2 lateral regions of the mandibular or distal tibial cartilage) were selected from each section.

A small group of pixels of positive staining (red for safranin O, and dark brown for DAB staining, respectively) was selected within each area by using the "magic wand" tool. Using "Similar" under the Selection command, the pixels were extended to regions containing color pixels of similar intensity. The data of the image histogram (mean intensity and pixel number of the selected color) were exported to Microsoft Excel. The image was then converted to grayscale, and the gray pixel values of the histogram of the entire field (total pixels) were also exported to Excel.

The percentage of the stained pixels, relative to the total pixels of each area, was calculated by dividing the selected color pixels by the total (gray) pixels of the entire area, and then multiplying by 100. By using the same main color intensity values for all tissue sections stained with the same reagent, quantitative comparison of positively stained areas of control and of arthritic specimens was carried out.

Average of data from left-side and right-side joints from the same mouse was handled as a single value from a single animal.

Quantitative real-time polymerase chain reaction (QRT-PCR)

Mandibular cartilage and adjacent synovial tissue (without bone) of wild-type and RA mice were dissected from euthanized animals (experimental groups similar to those shown in Fig. 1) under a preparative stereo microscope in RNAse-free conditions to isolate RNA. RNALater solution is used for collection of the tissue pieces were collected in and homogenized in TRI Reagent (Sigma-Aldrich). Tissue samples from at least two animals (4-6 TMJs) per group

(non-arthritic controls, mice with acute PGIA and mice with chronic PGIA) were pooled, and RNA was isolated from three independent pools. RNA was also isolated similarly from normal and inflamed paw homogenates, which contained cartilage and soft tissue dissected from the ankle and mid-foot area, but not bone. The quality of RNA samples was checked using an Agilent 2100 Bioanalyzer (Agilent Technologies, Foster City, CA). High quality samples were used in reverse transcription reactions. cDNAs were synthesized using an oligo-dT reverse primer and the SuperScript First Strand Synthesis kit (Invitrogen, Carlsbad, CA). QRT-PCR was carried out with the iQ5 real-time PCR detection system (Bio-Rad, Hercules, CA). Gene-specific PCR primers and FAM-labeled TaqMan probes for mouse IL-1β, stromelysin [MMP-3], ADAMTS-4 and ADAMTS-5 were purchased from Applied Biosystems (Foster City, CA).

According to the manufacturer's instructions (Applied Biosystems) TaqMan gene expression assays were carried out. QRT-PCR data were analyzed with the iQ5 system's software package. To normalize the data within each pooled sample, expression of the GAPDH housekeeping gene was used. Quantification of gene expression among pooled samples (relative to control) was done employing the $2^{-\Delta\Delta CT}$ method and results were expressed as fold changes relative to the corresponding control samples (43).

Statistical analysis

Statistical analysis was performed using SPSS software (version 16; SPSS Inc., Chicago, IL). Descriptive statistics were used to determine group means and 95% confidence intervals (mean ± CI 95%). Statistically significant differences among the groups were assessed using ANOVA with post-hoc Dunnett's t test for comparison of multiple groups. Two-tailed Pearson-correlation analysis was used to find correlations between data sets. A p value of <0.05 was considered statistically significant.

Study 2

Mice were immunized and assessed for arthritis as described in study 1.

Preparation of synovial fluid and tissue extracts

Immediately after euthanasia, synovial fluid was harvested from arthritic ankle joints (with the highest arthritis score of 4 in 20 µl of PBS/joint and centrifuged at 5,000 rpm for 10 min, and the supernatant was stored at −70 °C until use (44). Skin from paws of normal and arthritic mice was removed for tissue extracts preparation, Ankle and tarso-metatarsal joint (including bone) soft tissues were dissected and placed in cold radioimmune precipitation assay lysis buffer containing Halt protease inhibitor mixture (both from Pierce). Homogenates were prepared by ultrasonication (Virsonic Digital 50, VirTis, and Gardiner, NY) for 90 seconds on ice and centrifuged at 5,000 rpm. Measurement of the protein content of the supernatant of tissue extracts were done by using the bichinconic acid assay (Pierce).

Histology, histochemistry and IHC

For frozen section IHC, after euthanasia paws with similar degrees of arthritis were embedded in optimal cutting temperature medium, frozen, and sectioned with a tungsten knife at −32 °C in a MICROM HM 550 cryostat (MICROM International, Walldorf, Germany). Frozen sections were immunostained with mAbs to TSG-6 or goat Abs to mouse tryptases mMCP-6 and mMCP-7. Non-immune goat or mouse IgG served as a background control.

Reagents and cell culture

Chemicals were obtained from Sigma-Aldrich or Fisher, and molecular biology grade reagents were from Invitrogen. Recombinant human TSG-6 and rmTSG-6, rmMCP-6 and rmMCP-7 were obtained from R&D Systems (Minneapolis, MN), and cytokine ELISAs were from either BD Biosciences or R&D Systems. Horseradish peroxidase (HRP)-conjugated polyclonal antibodies (Abs) against murine IgG and IgG2a and HRP-labeled rabbit anti-goat IgG were purchased from BD Biosciences. Goat polyclonal Ab to murine HC1 and HC2 were

obtained from Santa Cruz Biotechnology, Inc. (Santa Cruz, CA), and goat Abs to mMCP-6 and mMCP-7 were from R&D Systems. Chinese hamster ovary (CHO-K1) cells were purchased from the American Type Culture Collection (ATCC; Manassas, VA), and murine CD44-transfected CTLL-2 cells (CTLL-2/CD44$^+$) were kindly donated by Robert Hyman (37). Unless noted otherwise, the standard cell culture medium was DMEM, containing 4.5 g/liter glucose and supplemented with 1% non-essential amino acid solution, 1 mM sodium pyruvate, 1% L-glutamine, 100 mg/liter gentamicin sulfate, 0.5 μM β-2-mercaptoethanol, and 10% FBS (fetal bovine serume, Hyclone, Logan, UT). All cell cultures were performed in a humidified atmosphere of 5% CO_2 in air at 37 °C.

Production and purification of rmTSG-6 fusion protein

A 753-bp-long cDNA fragment of mouse IgG2a heavy chain was obtained by reverse transcription of RNA purified from a mAb-producing murine B-cell hybridoma. The cDNA fragment was amplified by PCR using primers with linkers for restriction enzyme (EcoRI and BclI) cleavage sites. The 5′-end of the cDNA included the hinge region of the mouse IgG2a heavy chain, and it was inserted into a Lonza pEE14.1 mammalian expression vector (Lonza Biologics Ltd., Slough, UK) (Fig. 2A). The stop codon of the full-length (828-bp) mouse TSG-6 cDNA(38) in a pBlueScript S/K vector (Stratagene, La Jolla, CA) was replaced with a sequence coding for the cleavage site of the endopeptidase factor Xa (*Ile-Glu-Gly-Arg*) followed with a 9-bp spacer before the **EcoRI** cleavage site (*ATAGAAGGTCGT*/GACTCGAGG/**GAATTC**) at the 3′-end of the TSG-6 cDNA. Purified mTSG-6 cDNA was inserted into the EcoRI site between the Lonza vector and the 5′-end of the mouse IgG2a heavy chain (Fig. 2A). Insert orientation was determined by PCR, and the construct was sequenced. Semiconfluent CHO-K1 cells were transfected with the *mTSG-6-Xa-mFc2a*Lonza construct using $CaCl_2$ precipitation according to a standard protocol (39)

Figure 2.

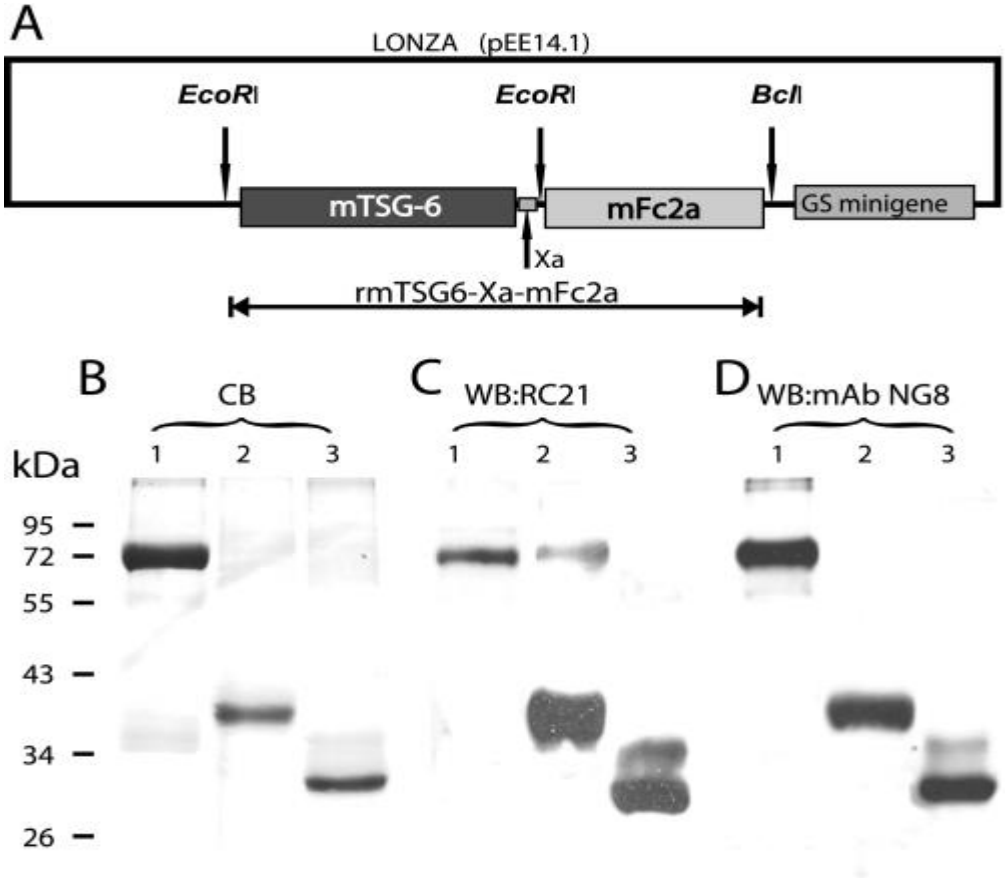

Figure 2. Schematics of the mammalian expression vector containing the rmTSG-6 fusion protein and analysis of purified rmTSG-6. (*A*), structure of the mammalian expression vector (Lonza pEE14.1-rmTSG-6-Xa-mFc2a) incorporating the fusion protein. Shown is detection of rmTSG-6 by SDS-PAGE and Coomassie Blue (*CB*) staining **(*B*)** and Western blotting (*WB*) with affinity-purified and biotinylated RC21 polyclonal rabbit anti-TSG-6 antibody **(*C*)** and monoclonal mouse anti-TSG-6 antibody (clone NG8) (*D*). The lanes were loaded with rmTSG-6 in the same order. *Lane 1*, the 72-kDa rmTSG-6-Xa-mFc2a fusion protein purified from CHO serum-free medium (a CHO line transfected with pEE14.1-rmTSG-6-Xa-mFc2a and cloned as described); *lane 2*, purified rmTSG-6 (~39 kDa without the mFc2a-tail) after factor-Xa cleavage and repurification on protein G-Sepharose; *lane 3*, the same rmTSG-6 as shown in*lane 2* but after deglycosylation (~30 kDa) using a kit containing peptide:*N*-glycosidase F, *O*-glycosidase, sialidase, β-galactosidase, and glucosaminidase. *B*, the TSG-6 proteins were loaded on 12% SDS-PAGE (20 µg protein/lane), run under reducing conditions and stained with Coomassie Blue (*CB*). *C* and *D*, the separated proteins (1 µg/lane) were transferred to nitrocellulose membrane and probed with biotinylated RC21 and NG8 antibodies, respectively, followed by HRP-streptavidin. Molecular mass is indicated in kDa. *WB*, Western blot.

The Lonza expression vector contains a minigene encoding glutamine synthase, an enzyme responsible for the biosynthesis of glutamine (using glutamate and ammonia as substrates). The transfected glutamine synthase gene (a part of the Lonza vector) can act as a selection tool in the presence of methionine sulfoximine, and CHO cells containing the Lonza vector with the glutamine synthase gene can survive in the absence of glutamine and in the presence of 25–50 μM methionine sulfoximine. Approximately 2 weeks after the transfection, individual CHO colonies were transferred into 96-well cell culture plates. Glutamine-free DMEM was replaced with CHO serum-free medium (Lonza Inc., Mapleton, IL), and 48 h later, 100 μl of supernatant from each well was transferred to 96-well Maxisorp ELISA plates (Nunc International, Hanover Park, IL) and incubated overnight. Free binding sites of the wells were blocked with 1% BSA, and the clones expressing the fusion protein (TSG-6-mFc2a) were identified with HRP-conjugated goat anti-mouse IgG2a. Positive colonies were retested using affinity-purified and biotinylated RC21 rabbit Ab raised against mouse TSG-6 (40-41-42) followed by incubation with HRP-labeled streptavidin and tetramethylbenzidine substrate (TMB; BD Biosciences OptEiA TMB substrate set). Cell lines secreting the highest amounts of fusion protein were cloned using the limiting dilution (0.5 cell/well) method and cultured in the presence of irradiated (70 grays) mouse embryonic fibroblast feeder cell layers. Positive colonies (retested by ELISA as described above) were recloned by limiting dilution, and stable clones, secreting high amounts of fusion protein, were subjected to further testing.

The rmTSG-6-Xa-mFc2a fusion protein from the serum-free supernatant of the CHO transfectant (clone 514) was purified on Protein G-Sepharose 4 Fast Flow (GE Healthcare) according to the manufacturer's instructions. The eluted product was dialyzed against ultrapure H_2O, lyophilized, and stored at −20 °C until further use. The purity of the fusion protein was determined using SDS-PAGE with Coomassie Blue staining. Western blots were performed with HRP-labeled goat anti-mouse IgG2a or with affinity-purified and biotinylated rabbit RC21 anti-TSG-6 antibody (42). Purified rmTSG-6-Xa-mFc2a fusion protein was cleaved with factor Xa (200 units/mg protein) in 2.5 ml of factor Xa cleavage/capture buffer (Novagen, Madison, WI) (100 mM NaCl, 50 mM Tris-HCl, 5 mM $CaCl_2$,

pH 8.0) overnight at room temperature. The enzyme was removed by XarrestSepharose (Novagen), and the IgG2a-Fc fragment was absorbed onto Protein G-Sepharose.

After optimization of factor Xa cleavage, we tested the glycosylation level of purified rmTSG-6 (clone 514). Twenty µg of purified protein was digested using a deglycosylation kit (Enzymatic DeglycoMx kit; QA-Bio LLC, Palm Desert, CA) containing a mixture of peptide:*N*-glycosidase F, *O*-glycosidase, sialidase, β-galacosidase, and glucosaminidase, which removed all *N*-linked and most of the *O*-linked oligosaccharides. The digested product was loaded on 12% SDS-PAGE and transferred onto nitrocellulose membrane for immunostaining as described above.

Testing of HA binding and enhancement of HA-CD44 interaction by rmTSG-6

Binding of rmTSG-6 to immobilized HA or heparin was tested using a microplate titration assay (Fig 3*A* and *B*). In brief, rooster comb HA (Sigma) was serially diluted in PBS (from 200 µg/ml to 3.1 µg/ml). One hundred µl of each HA solution was dispensed into duplicate wells of 96-well Maxisorp plates and incubated overnight at room temperature. Free binding sites were blocked with 1% BSA. rmTSG-6 (from clone 514, free of IgG-Fc tail) was diluted in PBS (concentration range, 0.031–2.0 µg/100 µl per well) and incubated with the HA-coated wells for 2 h at 37 °C. HA-bound rmTSG-6 was detected with biotinylated RC21 antibody, followed by HRP-streptavidin and TMB substrate. rmTSG-6-mediated enhancement of HA binding to cell surface CD44 was tested using murine CTLL-2/CD44$^+$ cells (35) Relative amounts of cell surface-bound fluorescein-conjugated HA (FL-HA) in the presence or absence of rmTSG-6 were measured by flow cytometry as described before (33).

Briefly, HA-rmTSG-6 complex was formed by incubating FL-HA with rmTSG-6 at a 5:1 ratio (w/w) in PBS (pH 7.2) for 30 min at room temperature. The solution containing this complex was then added to CTLL-2/CD44$^+$ cells and incubated for 1 h at 4 °C. Base-line HA binding was determined by incubating the cells with the same amount of FL-HA alone, and PBS alone served as the background control. Cell surface fluorescence was detected and analyzed using a FACSCalibur flow cytometer and CellQuest software (BD Biosciences) (33) (Fig. 3*C*).

TSG-6-specific monoclonal antibody (mAb) production and development of capture Enzyme-Linked ImmunoSorbent Assays (ELISA*)*

RmTSG-6 has been used to immunize TSG-6-deficient BALB/c mice, in order to generate murine B cells for hybridoma fusion and subsequent TSG-6-specific mAb production (34) (Mice from The Jackson Laboratory; stock number 012903). Animal experiments were all approved by the Institutional Animal Care and Use Committee of Rush University Medical Center (Chicago, IL). Immunization of TSG-6-deficient BALB/c mice were done by intraperitoneal injection with 50 μg of purified rmTSG-6 emulsified with 2 mg of dimethyldioctadecyl-ammonium bromide (DDA) adjuvant in a total volume of 100 μl of PBS. After the third injection, the peripheral blood samples were collected, and anti-TSG-6 serum titers were determined by ELISA (using immobilized rmTSG-6 as the antigen and HRP-conjugated anti-mouse IgG for detection). Following the standard protocol, we fused Spleen cells from positive mice with the Sp2/0-Ag14 myeloma cell line (ATCC) and selection of the mAb-producing hybridomas were done by ELISA (45, 46). Positive hybridomas were repeatedly Cloned by limiting dilution, and after hybridoma injection, ascites fluid was produced in BALB/c mice. By using a mouse IgG isotype determination kit (Santa Cruz) we could identify the isotypes and light chains of each mAb.The purification of the Immunoglobulin fractions of five hybridoma clones (designated NG2, NG3, NG4, NG5, and NG8) were done on protein G columns, and by using a standard inhibition ELISA a portion of each was biotinylated and tested for cross-reactivity(46). In brief, 0.1 μg of rmTSG-6 was coated to each well, and serial dilutions of purified anti-TSG-6 mAbs were mixed with optimally diluted aliquots of each biotinylated anti-mTSG-6 mAb.

As additional positive controls, rmTsg-6 mouse and human TSG-6 proteins (R&D Systems) were used and for the in-house development of new murine and human TSG-6 capture ELISA systems employing non-cross-reactive pairs of anti-TSG-6 mAbs. For the capture of either murine or human TSG-6 Purified mAb NG3 (IgG2b κ) was used.

For the detection of murine TSG-6 Biotinylated NG8 mAb (IgG1 κ) was employed, and for the detection of human TSG-6 (an example of the standard curve of murine TSG-6 ELISA is shown in Fig. 3*D*) NG4 (IgG1 κ) was used.

The sensitivity of capture ELISAs ranged from 500 pg/ml to 200 ng/ml TSG-6.

Figure 3.

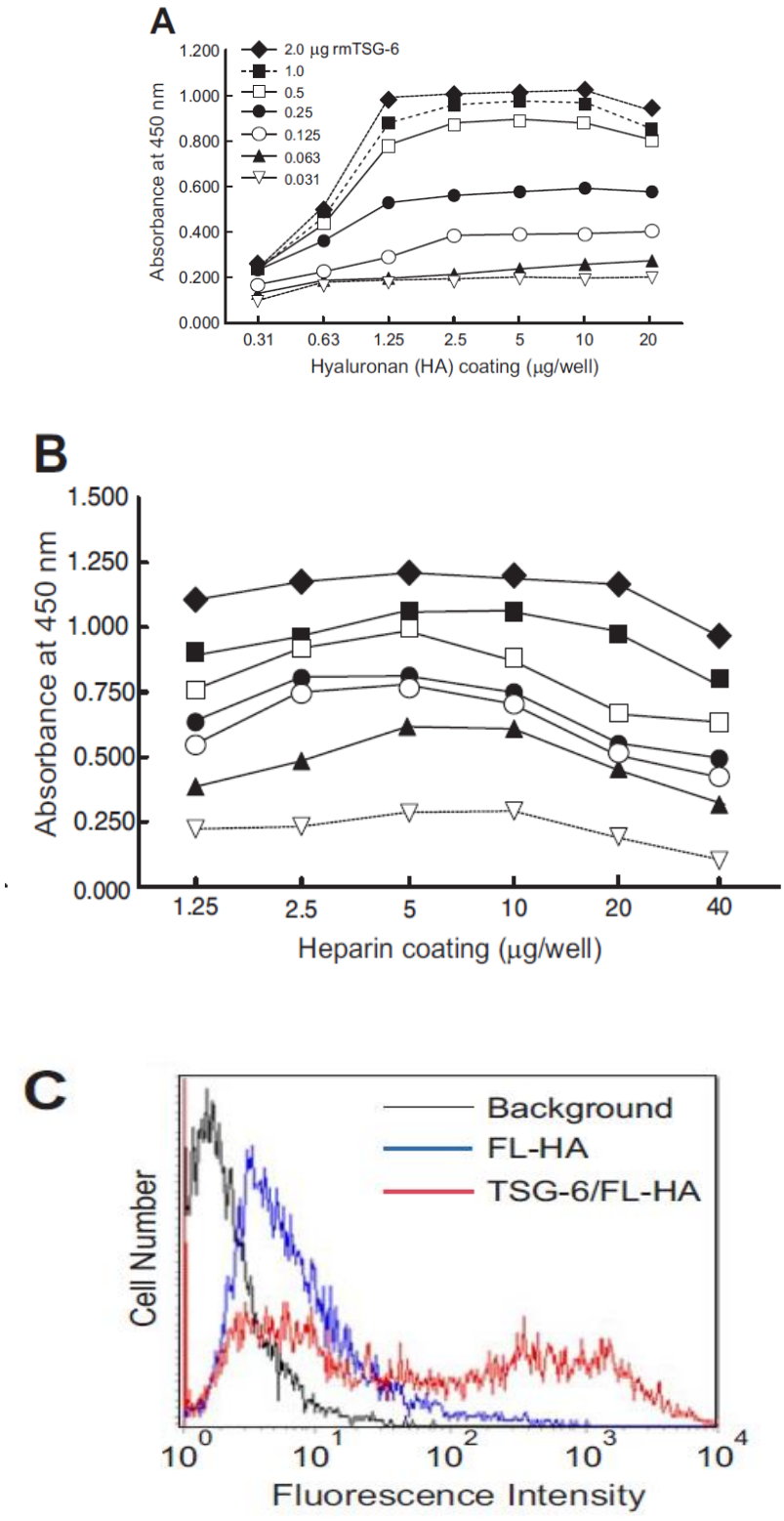
A
2.0 µg rmTSG-6
1.0
0.5
0.25
0.125
0.063
0.031
Absorbance at 450 nm
1.200
1.000
0.800
0.600
0.400
0.200
0.000
0.31
0.63
1.25
2.5
5
10
20
Hyaluronan (HA) coating (µg/well)
B
Absorbance at 450 nm
1.500
1.250
1.000
0.750
0.500
0.250
0.000
1.25
2.5
5
10
20
40
Heparin coating (µg/well)
C
Background
FL-HA
TSG-6/FL-HA
Cell Number
10^0
10^1
10^2
10^3
10^4
Fluorescence Intensity

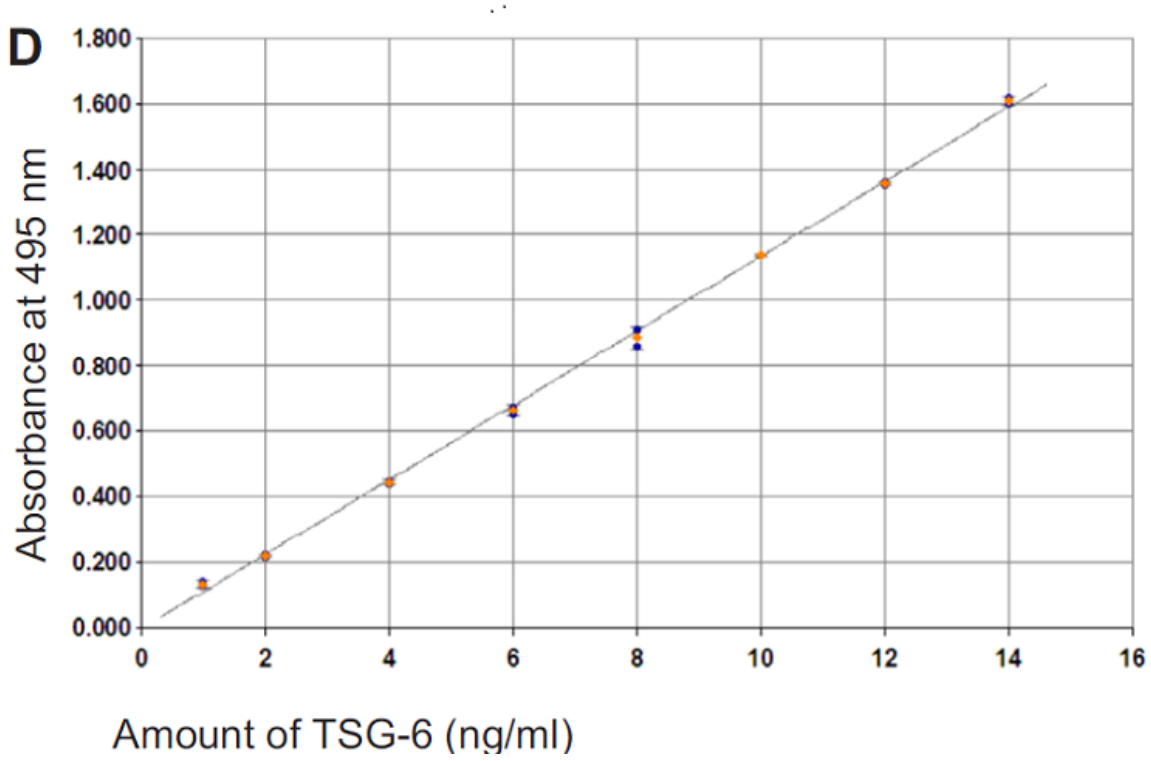

Figure 3. Measurement of the hyaluronan (HA) and heparin binding functions of TSG-6 and example of a standard curve of murine TSG-6 ELISA. (A) Binding of rmTSG-6 to immobilized HA was titrated in a microplate assay. Saturation was achieved at or above 1 μg/well rmTSG-6 in wells coated with 1.25 to 20 μg HA. (B) Binding of rmTSG-6 to immobilized heparin was titrated in a microplate assay. Saturation was achieved at or above 1 μg/well rmTSG-6 in wells coated with 1.25 to 20 μg HA. One of 2 experiments (with similar results) is shown. (C) Enhancement of HA binding to cell surface CD44 was tested using murine CD44-transfected CTLL- 2 lymphoma cells. The cells were reacted with fluorescein-labeled HA (FL-HA) or pre-formed complexes of rmTSG-6 and FL-HA as described in the Experimental Procedures. Cell surface-bound FL-HA was detected by flow cytometry. Background staining (autofluorescence) is indicated with a black histogram; binding of FL-HA alone and of the TSG-6/FL-HA complex are depicted with blue and red histograms, respectively. (D) A typical standard curve of the murine TSG-6 ELISA. NG3 anti-TSG-6 mAb was used for capture, and biotinylated NG8 mAb for detection. The concentrations of rmTSG-6 are indicated on the x axis.

In vitro detection of interactions of TSG-6 with HA or heparin and mast cell tryptases

In preliminary experiments, optimal concentrations of rooster comb HA or heparin (both from Sigma); rmTSG-6, rmMCP-6, and rmMCP-7; and Abs against TSG-6 and mMCP-6 and mMCP-7 were determined for the detection of HA- or heparin-bound proteins (TSG-6 and the mast cell tryptases mMCP-6 and mMCP-7), by employing ELISA-based systems.

For detection of a tripartite interaction of HA or heparin with TSG-6 and tryptases, a triple layer sandwich microplate assay were developed. Briefly, overnight coating at room temperature is done with 2 μg of HA in 100 μl of PBS (first layer) onto the wells of Maxisorp (Nunc) plates. Overnight coating of Heparin (10 μg) in 1% *N*-(3-dimethylaminopropyl)-*N*-ethyl-carbodiimide hydrochloride which was dissolved in H_2O and added onto the wells of CovaLink (Nunc) plates at 37 °C (47).

Blocking of the free binding sites was done with 5% BSA, then wells were filled with 0.1 μg of rmTSG-6 (second layer) and incubated for 1 h at 37 °C, followed by incubation with rmMCP-6 or rmMCP-7 (third layer; concentration range, 0.025–0.2 μg/well). Detection of the third layer of bound tryptases was done with anti-mMCP-6 and anti-mMCP-7 Abs.

RmMCP-6 or rmMCP-7 was used as a second layer, and rmTSG-6 was used as the third layer (at the concentrations described above), followed by detection of bound rmTSG-6 with biotinylated NG8 mAb.

Reference wells contained only a single protein (TSG-6 or tryptase) in each assay, and detection of the immobilized proteins was done with the irrelevant Ab (rmTSG-6 with anti-tryptase Abs and *vice versa*) which served as background controls. Development of the reactions was done with HRP-conjugated secondary reagents and TMB substrate, and values were expressed as the absorbance measured at 450 nm using a Synergy 2 ELISA reader (BioTek Instruments, Winooski, VT).

Identification of mast cell tryptases by Western blotting and co-immunoprecipitation of tryptases and HCs of IαI with TSG-6

As described earlier tissue extracts were prepared from arthritic and non-arthritic paws, and 50 μg protein of each was loaded onto 12% SDS-PAGE, along with 0.2 μg of rmTSG-6, 0.1 μg of rmMCP-6, and 0.05 μg of rmMCP-7. Under reducing conditions the proteins were resolved, and transferred to a nitrocellulose membrane, and probed with different antibodies: affinity-purified biotinylated rabbit RC21 anti-TSG-6 Ab, anti-MCP-6, or anti-MCP-7.

In most cases, we stripped the membranes and reprobed them with another antibody to detect comigration of the two proteins. With or without immunoprecipitation the supernatants of paw extracts were subjected to Western blotting as described (35, 48) .

We preabsorbed the supernatants of paw extracts (200 μg of protein of each) with Protein G-Sepharose for co-immunoprecipitation, washed, and then incubated them overnight at 4 °C on a rotary shaker, with 10 μg of TSG-6 mAb mixture (NG3, NG4, NG5, and NG8; 2.5 μg of each) Immune complexes were absorbed to Protein G-Sepharose for 30 min at room temperature, washed, and boiled in reducing buffer. We loaded 1/3 of each sample on 12% SDS-PAGE, and under reducing conditions proteins were separated. Transferring of the Proteins were done onto nitrocellulose membrane and staining was done with biotinylated Abs to TSG-6 (RC21 or NG8) or with goat antibodies to HC1 or HC2 (both at 1:500 dilution) or goat antibodies to mMCP-6 or mMCP-7 (both at 1:2,000 dilution) followed by HRP-conjugated rabbit antibody to goat IgG (Invitrogen; 1:5,000 dilution).

In order to ensure that equal amounts of cell extracts were loaded HRP-labeled mouse mAb to β-actin (Invitrogen; 1:5,000 dilution) was used. All incubations were performed at room temperature for 1–2 h. Detection of the positive protein bands were done by ECL (Amersham Biosciences).

Statistical analysis was performed using SPSS as described in study 1.

Results

We examined and evaluated TMJ involvement in PGIA in the acute (10 mice) and subacute/chronic (12 mice) phases of peripheral joint inflammation compared with age-matched, (8 PBS/DDA-injected) non-arthritic, control animals. After the third injection of PG in (DDA) [Fig. 1A (thick solid arrow)] arthritis developed. This initial acute phase [Fig. 1A, dotted-line arrow)] was characterized by increased swelling and redness of the paws. Mice entered the chronic phase of PGIA [Fig. 1A, dashed-line arrow] around 10 days after arthritis onset (~day 52 of immunization), which can be characterized by hardening of the periarticular soft tissue, deformities and ankylosis (19, 38).

On day 60 which is the end of the experimental period, 11 of the 12 remaining PG-immunized animals had chronic arthritis involving the limbs, although none of the control animals showed any signs of joint disease [Fig. 1A-B]. Mice with acute and chronic arthritis were sacrificed on days 49–50 and day 60, respectively [Fig. 1A (thin solid arrows)] to monitor the progression of inflammation or cartilage destruction in the TMJs (if any), we compared their TMJs and ankle joints with each other or with the corresponding tissues of non-arthritic control mice. Figures 4A and 4B show representative examples of hematoxylin-eosin-stained (HE) histological sections prepared from the ankle joints of control and arthritic animals sacrificed on day 60. The ankle joints of the control mice did not exhibit any signs of structural damage [Fig.4A], but inflammatory cell infiltration of the synovial tissue and massive joint destruction was evident in the ankles of the PG-immunized animals [Fig. 4B]. The extent of inflammation-induced loss of cartilage aggrecan was determined with staining of adjacent sections of the ankle joints of normal and arthritic mice with safranin O and fast green.

Safranin O can detect the negatively charged glycosaminoglycans (GAG's) side chains of aggrecan in cartilage. Accordingly, the extent of red staining is proportional to the amount of GAG-containing (presumably intact) aggrecan molecules (39).

Intense red staining with safranin O could be seen on cartilage of the distal tibia of the control mouse [Fig. 4(A1)], although very little red staining was seen in the tibial cartilage of the mouse with chronic arthritis in the ankle joint [Fig. 4(B1)]. We were investigating to determine whether the aggrecanneoepitopes generated by ADAMTSs or MMP-3 (-NITEGE and -VDIPEN, respectively) were detectable in the cartilage of arthritic ankles by considering that the loss of GAG-decorated aggrecan fragments from cartilage is the result of cleavage of the core protein by aggrecanases (ADAMTS-4 and ADAMTS-5) or stromelysin (MMP-3) (40, 49). As compared to the normal cartilage, which showed essentially negligible immunostaining with the anti-NITEGE antibody [Fig.4(A2)], staining for this aggrecanneoepitope was very strong in the cartilage of arthritic ankle [Fig. 4(B2)]. Similar differences could be seen when sections of control and arthritic ankle joints were reacted with the anti-VDIPEN antibody [Table I and results not shown].

Figure 4.

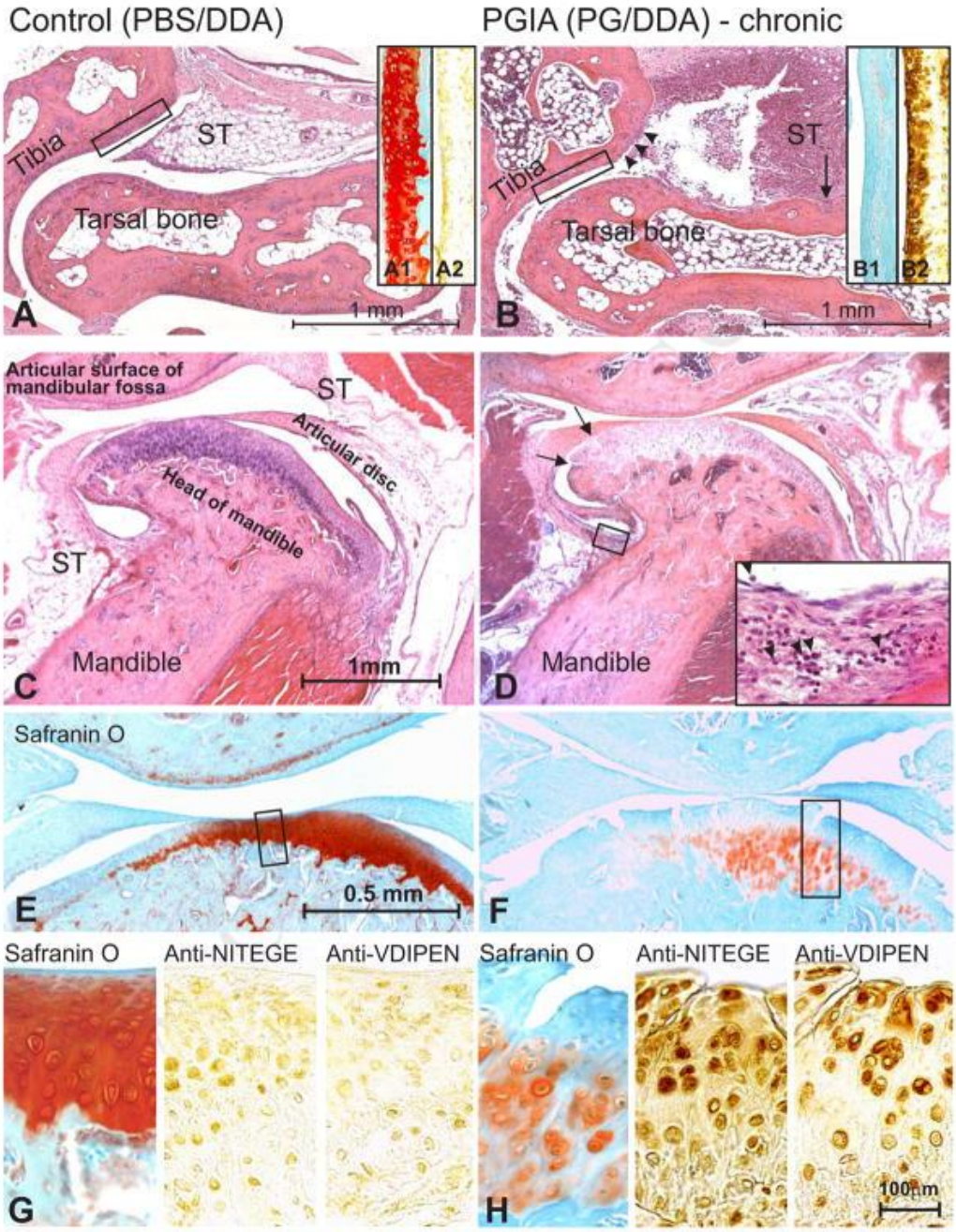

Histochemical and immunohistochemical features of the limb (ankle) joints and temporomandibular joints (TMJ) in mice with proteoglycan induced arthritis.

(A) A hematoxylin-eosin-stained tissue section from the ankle (tibio-tarsal) joint from a PBS/DDA injected control mouse shows normal structure. The articular cartilage surface is smooth, and the synovial tissue (ST) is free of inflammatory cell infiltrates.
(**A1**) The articular cartilage of the distal tibia (section adjacent to the boxed area in A) shows strong and fairly even staining with safranin O (red), but (**A2**) negligible immunostaining for aggrecanneoepitopes with anti-NITEGE antibody (or anti-VDIPEN; not shown).

(B) The ankle joint from a mouse with chronic arthritis shows massive infiltration of synovial tissue (ST) by leukocytes and loss of superficial zone chondrocytes at the joint margins where inflammatory cells

are in contact with cartilage (also known as “pitting”; depicted here by arrowheads). Bone erosion by the invasive synovium is also evident (arrow).
(**B1**) The cartilage of distal tibia shows generalized loss of safranin O staining, associated with (**B2**) strong positive immunostaining for aggrecanneoepitopes (anti-NITEGE is shown).
(**C**) Normal TMJ structure from the control mouse.
(**D**) The TMJ of the mouse with chronic PGIA (ankle shown in B). The TMJ does not exhibit severe structural damage, except for the lighter staining of the mandibular cartilage than the control TMJ, and a few fissures at the cartilage margin (arrows). A small collection of inflammatory cells is also present in the synovium (box and insert at 6x magnification).
(**E**) The cartilage of the normal TMJ shows strong and homogenous staining with safranin O (red), which indicates intact aggrecan content.
(**F**) Safranin O staining is weak and restricted to a few chondrocytes in the TMJ cartilage of a mouse with chronic PGIA. The cartilage also shows evidence of structural damage (fissures) and chondrocyte clustering (boxed area, magnified in H).
(**G**) Adjacent sections of the control TMJ were stained with safranin O (left-hand panel) and with antibodies against the aggrecanneoepitopes -NITEGE (middle panel) and -VDIPEN (right-hand panel). Weak positive staining for both neoepitopes is visible around some chondrocytes.
(**H**) The area of the TMJ from the arthritic mouse that stains weakly with safranin O (left-hand panel) shows strong immunostaining for both -NITEGE and -VDIPEN neoepitopes (middle and right-hand panels, respectively).

Table I. **Quantitative analysis of Safranin O staining of GAGs and immunohistochemical staining of aggrecanneoepitopes (NITEGE and VDIPEN) of the cartilage of TMJ and ankle joints in mice with acute or chronic PGIA and in non-arthritic controls**

Joint/Staining (% positive)	Control (N = 8)	Acute PGIA (N = 10)	p (acute vs. control)	Chronic PGIA (N = 11)	p (chronic vs. control)	p (chronic vs. acute)
TMJ/Safranin O						
Mean (CI 95%)	54.2 (46.2 – 62.2)	49.1 (43.0 – 55.2)	0.1911	6.4 (4.5 – 8.3)	*0.0014*	*0.0027*
Ankle/Safranin O						
Mean (CI 95%)	47.9 (40.6 – 55.2)	12.6 (9.3 – 15.9)	*0.0033*	1.9 (1.0 – 2.8)	*0.0001*	*0.0079*
TMJ/NITEGE						
Mean (CI 95%)	2.1 (1.6 – 2.6)	2.6 (1.8 – 3.4)	0.2565	16.7 (13.2 – 20.2)	*0.0299*	*0.0357*
Ankle/NITEGE						
Mean (CI 95%)	0.7 (0.3 – 1.1)	15.5 (11.7 – 19.3)	*0.0016*	26.3 (22.2 – 30.4)	*0.0004*	*0.0425*
TMJ/VDIPEN						
Mean (CI 95%)	0.5 (0.2 – 0.8)	1.1 (0.6 – 1.6)	*0.0450*	13.9 (10.3 – 17.5)	*0.0001*	*0.0003*
Ankle/VDIPEN						
Mean (CI 95%)	0.7 (0.2 – 1.2)	N.D.		19.0 (14.7 – 23.3)	*0.0001*	

The percent of positively stained area (% positive) within each TMJ or ankle cartilage section was quantitatively determined using Adobe Photoshop-based image analysis, as described in the Methods. The values shown are the means and 95% confidence levels (CI 95%). Statistically significant differences ($p<0.05$) are indicated in italics. N: number of mice; N.D.: not determined.

After comparing hematoxylin and eosin (HE) stained sections of the TMJs from control and arthritic mice, prominent difference was the diminished basophilic staining in the mandibular cartilage of arthritic mice [Fig. 4(C) and (D)]. Structural evidence of cartilage damage (fibrillation or fissures) the TMJ [Fig. 4 (D, arrows), or small collections of inflammatory cells could be seen in the TMJ synovium [Fig. 4 (D, insert)] in the most severe cases of chronic PGIA. Adjacent sections of the corresponding TMJs were stained with safranin O and fast green to be able to determine if in the apparent loss of hematoxylin staining from the TMJ cartilage of the arthritic mouse could reflect a loss of aggrecan. Indeed, the control TMJ cartilage showed strong and nearly homogenous staining with safranin O [Fig. 4(E) and (G)] whereas significant loss of red staining was observed in the TMJ of the arthritic mouse [Fig. 4(F) and (H)]. In the latter case, safranin O staining could be seen around the chondrocytes mainly and was absent from the inter-territorial matrix. In addition, the chondrocytes appeared to form clusters in the TMJ of the arthritic mouse [Fig. 4(H)].

Immunostaining for aggrecan neoepitopes showed light staining for both -NITEGE and -VDIPEN around some of the chondrocytes in the healthy TMJ [Fig.4 (G, middle and right-side panels, respectively)], which is consistent with the normal turnover of aggrecan in the cartilage. In comparison with the control mice, immunostaining for -NITEGE and -VDIPEN was very strong in the TMJ cartilage of the arthritic mouse [Fig. 4(H)], which indicated that aggrecan fragments were generated more extensively in the TMJ of the mouse affected with peripheral joint inflammation than in the control mice without arthritis.

While the presence of inflammatory cells in the TMJs was not typical, diminished safranin O staining and enhanced aggrecan neoepitope immunostaining could be seen in the TMJs of most animals at the chronic phase of PGIA and in a few TMJs in the acute arthritic group. Morphometric analyses of safranin O staining and IHC (anti-NITEGE and anti-VDIPEN) reactions were performed to quantitatively assess the extent of aggrecan degradation in the different joints by using tissue sections from the TMJ and ankle joints of control mice and of animals with acute and chronic PGIA. As shown in Table I, neither safranin O staining nor immunostaining for the NITEGE neoepitope in the TMJ cartilage was significantly different between normal mice and those with acute proteoglycan induced arthritis, but after the mice reached the chronic phase of PGIA the differences became statistically significant. In the

arthritic ankle joints, aggrecan degradation (diminished safranin O staining and generation of NITEGE neoepitope) was significantly greater than in the controls already at the acute phase of PGIA, and progressed further in chronic disease [Table I].

These results indicated that aggrecan degradation occurred in both the ankles and the TMJs in PGIA, but was more progressive in the ankles than in the TMJ.

The absence of synovial inflammation or presence of very little inflammation coupled with massive loss of aggrecan is one of the typical features of osteoarthritis (50).

Pro-inflammatory cytokines, such as IL-1β, TNFα, IL-6, or IL-17, have been implicated in the initiation of matrix breakdown in cartilage (50, 51). Among these cytokines, IL-1β, which can also be produced by the chondrocytes themselves in osteoarthritis (OA), is thought to be the main effector of aggrecan breakdown *via* induction of aggrecanase and MMP expression in the chondrocytes (51). Evidence of upregulated expression of the genes encoding ADAMTS-4, ADAMTS-5 and MMP-3 (~20-fold, ~7-fold, and ~18-fold increases, respectively, relative to normal controls) in the TMJs of animals with both acute and chronic proteoglycan induced arthritis [Figs 5(A-C)] could be found, but the IL-1β gene was not upregulated (only ~1.5-fold higher than control) in these TMJ samples [Fig. 5(D)]. As inflammation progressed the expression levels of aggrecanases and MMP-3 in the arthritic peripheral joints increased [Figs 5(E, F, G)], but the overall magnitude of gene expression was similar to the levels found in the TMJ; except for ADAMTS-5, which was expressed at slightly lower levels in the arthritic ankle joints.

In contrast, the IL-1β gene was highly over-expressed in the arthritic limbs at both the acute and the chronic phases of proteoglycan induced arthritis relative to the normal control, although there was a statistically significant decrease in expression as arthritis progressed into the chronic phase [Fig. 5(H)].

This latter observation suggested that the inflamed limb joints were the major sources of the "catabolic" cytokine IL-1β.

Figure 5.

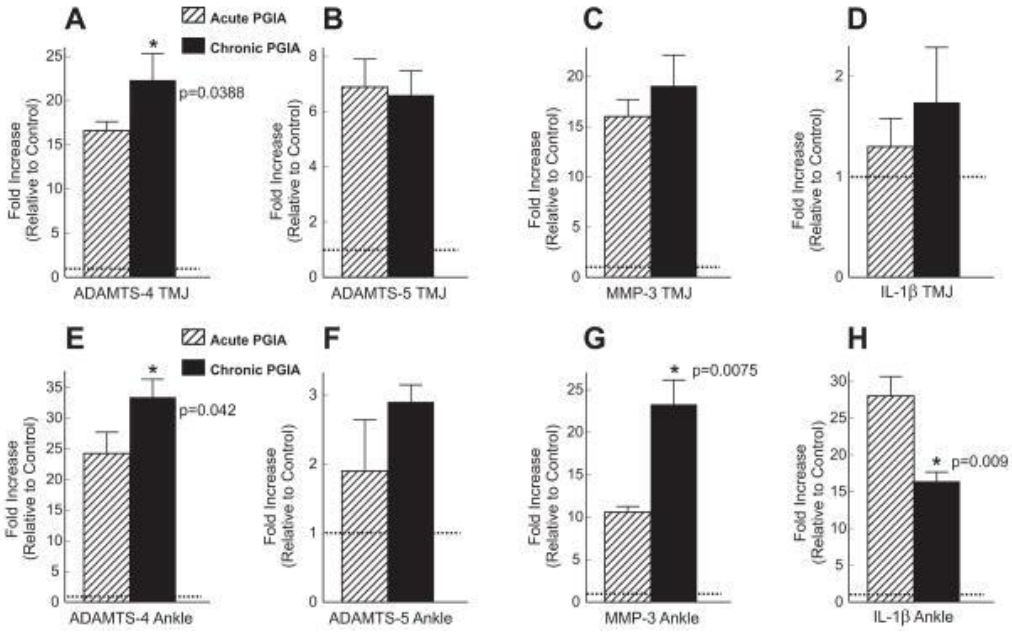

Figure 5. Expression of genes encoding matrix-degrading enzymes and interleukin (IL)-1β in the TMJs and ankle joints of mice with PGIA. Quantitative real-time PCR (qRT-PCR) was employed to compare the expression levels of these genes between control and arthritic mice in the TMJs (**A–D**) and the ankle joints (**E–H**) in PGIA. The results are from three independent experiments (N=3), using RNA of cartilage and synovial tissue (pooled from the joints of 2–3 mice per group), and are expressed as fold change (increase) in expression level relative to the control (mean ± 95% confidence interval). For comparison of the magnitude of gene upregulation, the control levels are indicated by horizontal dotted lines. Statistically significant differences ($p<0.05$) between "acute" and "chronic" PGIA samples are depicted by asterisks and the p values are indicated.
(**A**) The gene encoding the aggrecanase ADAMTS-4 was upregulated in the TMJs of mice with both acute (crossed bars) and chronic (black bars) arthritis compared to TMJs of non-arthritic mice (dashed line).
(**B**) The aggrecanase ADAMTS-5 was also upregulated, but to a lesser extent.
(**C**) Over-expression of MMP-3 (stromelysin) was also detected in the PGIA samples.
(**D**) The expression level of IL-1β in the TMJs of arthritic mice was only slightly above the level observed in control mice.
(**E**) ADAMTS-4 was highly upregulated in the arthritic joints at both the acute and chronic phases of PGIA.
(**F**) ADAMTS-5 was only marginally upregulated in the same joint samples.
(**G**) MMP-3 was moderately over-expressed in the joints of animals with acute PGIA and strongly over-expressed in animals with chronic disease.
(**H**) Conversely, IL-1β was massively upregulated in ankle joints with acute arthritis and moderately in those with chronic inflammation. The most notable difference between the TMJs and ankle joints was the very high level of IL-1β gene expression in the arthritic ankles (graph **H**) compared to the nearly normal levels in the TMJs (graph **D**) of corresponding groups of mice.

IL-1β needs to be present in the circulation to be able to act on the temporomandibular joint cartilage at an area that is distant from the sites of production. As expected, IL-1β could be detected in the sera of mice with either acute or chronic PGIA although could not be detected in the sera of control animals [Table II].

Moreover, additional pro-inflammatory cytokines, such as TNFα, IL-6, and IL-17, all of which could also contribute to cartilage matrix breakdown (56), were detected in the sera of arthritic animals at both the acute and chronic phases of PGIA [Table II].

Table II. Serum levels of pro-inflammatory cytokines in mice with acute or chronic PGIA and in non-arthritic controls

Cytokine (pg/ml)	Acute PGIA (N = 10)	Chronic PGIA (N = 12)	Control (N = 8)
IL-1β			
Mean (CI 95%)	9.5 (7.48 – 11.52)	9.31 (7.88 – 10.74)	0 (0)
TNFα			
Mean (CI 95%)	9.27 (8.01 – 10.53)	8.34 (6.63 – 10.05)	0 (0)
IL-6			
Mean (CI 95%)	17.5 (14.92 – 20.08)	14.3 (12.75 – 15.31)	0 (0)
IL-17			
Mean (CI 95%)	5.27 (4.06 – 6.48)	5.35 (4.64 – 6.06)	0 (0)

Serum levels of IL-1β, TNF-α, IL-6, and IL-17 are expressed in pg/ml. Values of the means and 95% confidence levels (CI 95%) are shown. None of these cytokines were detectable in serum samples of control (DDA adjuvant-injected, non-arthritic) mice (last column). The differences between mice with acute and chronic PGIA were not statistically significant in the serum levels of any of these cytokines ($p>0.05$). N: number of mice.

Production, purification, and cleavage of recombinant mouse TSG-6 (rmTSG-6) fusion protein

Our first aim of this study was to develop a simple expression system for high yield production of functionally active rmTSG-6.

The schematics of the construct used for CHO cell transfection can be seen on Fig.2A, we described the stepwise cloning method under "Experimental Procedures." Positive selection of transfectants, followed by a limiting dilution cloning procedure and a direct ELISA system using either a tag-specific (mouse IgG2a-Fc) or a protein-specific (TSG-6) Ab, allowed us to select clones with the highest yield of the fusion protein. Real-time PCR confirmed the presence of >80 copy numbers using the template of genomic DNA of the CHO transfectant, and ~0.8–1.2 mg of recombinant fusion protein could be purified from 100 ml of conditioned medium of clone 514.

The purity of the rmTSG-6-Xa-mFc2a fusion protein (~72 kDa) and rmTSG-6 (~39 kDa after cleavage with factor Xa and repurification on Protein G-Sepharose), were over 95%, although some degradation occurred during the enzymatic cleavage and repeated purification (Fig.2 B-D). Because rmTSG-6 was synthesized by CHO cells in serum-free medium, serum immunoglobulins and IαI could not affect the purity (*first* and *second lanes* in Fig.2B-D) or the functionality of secreted rmTSG-6. The molecular mass of purified rmTSG-6 after Xa cleavage was ~39 kDa (instead of ~30 kDa), indicating that the CHO cell-secreted rmTSG-6 was glycosylated (Fig.2B-D, *second lanes*). Indeed, enzymatic removal of all *N*-linked and most *O*-linked oligosaccharides reduced the mass of rmTSG-6 to the expected ~30 kDa size (*third lanes*, Fig.2B-D). The Fc-free rmTSG-6 was largely water-insoluble but could be solubilized by the addition of 5% BSA and dialysis against serum-free CHO medium. Purified rmTSG-6 bound HA in a concentration-dependent manner, and similar to recombinant human TSG-6**,** it enhanced the binding of fluorescence-labeled HA to cell surface CD44 (35)(Fig.3*C*). We used rmTSG-6 for immunization of TSG-6-deficient mice and subsequent generation of TSG-6-specific mAbs (clones NG2, NG3, NG4, NG5, and NG8). RmTSG-6 also served as a reference standard (Fig. 3*D*) for the development and use of mouse TSG-6 ELISA systems.

Serum TSG-6 concentrations correlate with arthritis severity and serum levels of pro-inflammatory cytokines but not with immune responses in PGIA

We used purified rmTSG-6 and optimally paired mAbs to be able to measure TSG-6 concentrations in serum and synovial fluid samples and in tissue extracts of inflamed joints of BALB/c mice immunized with cartilage PG on days 0, 21, and 42 to induce PGIA. By day 61 of immunization serum TSG-6 reached the maximum levels, around the time when the acute joint inflammation (swelling, redness, and cell infiltration) also reached the maximum (Fig. 6A and B). Although, whereas joint inflammation (arthritis score) declined slowly (Fig. 6A, solid diamonds), serum TSG-6 concentrations declined more rapidly (Fig.6A, *solid squares*). Low levels of TSG-6 could also be detected in the serum of PBS/DDA-injected mice (*open squares* in Fig. 6A), which was probably due to the activation of innate immune cells at the injection site (peritoneal cavity) (52).

Thus, the amount of TSG-6 in serum can be regarded as an indicator of pre inflammatory and inflammatory processes and appears to be a more reliable "biomarker" of the severity of acute disease than the levels of proinflammatory cytokines in PGIA(53) (Table 3). The correlation between arthritis score and serum TSG-6 was not significant at the early stage of disease (day 54) but became significant at the peak of arthritis (day 61) and remained such during progression toward chronic disease (Fig.6A and Table 3).

Although TSG-6 became undetectable in serum samples harvested from mice at late stages of PGIA (120–150 days after the first immunization), when acute synovial inflammation had given way to pathologic joint remodeling, it lead to deformities and loss of function (data not shown).

Figure 6.

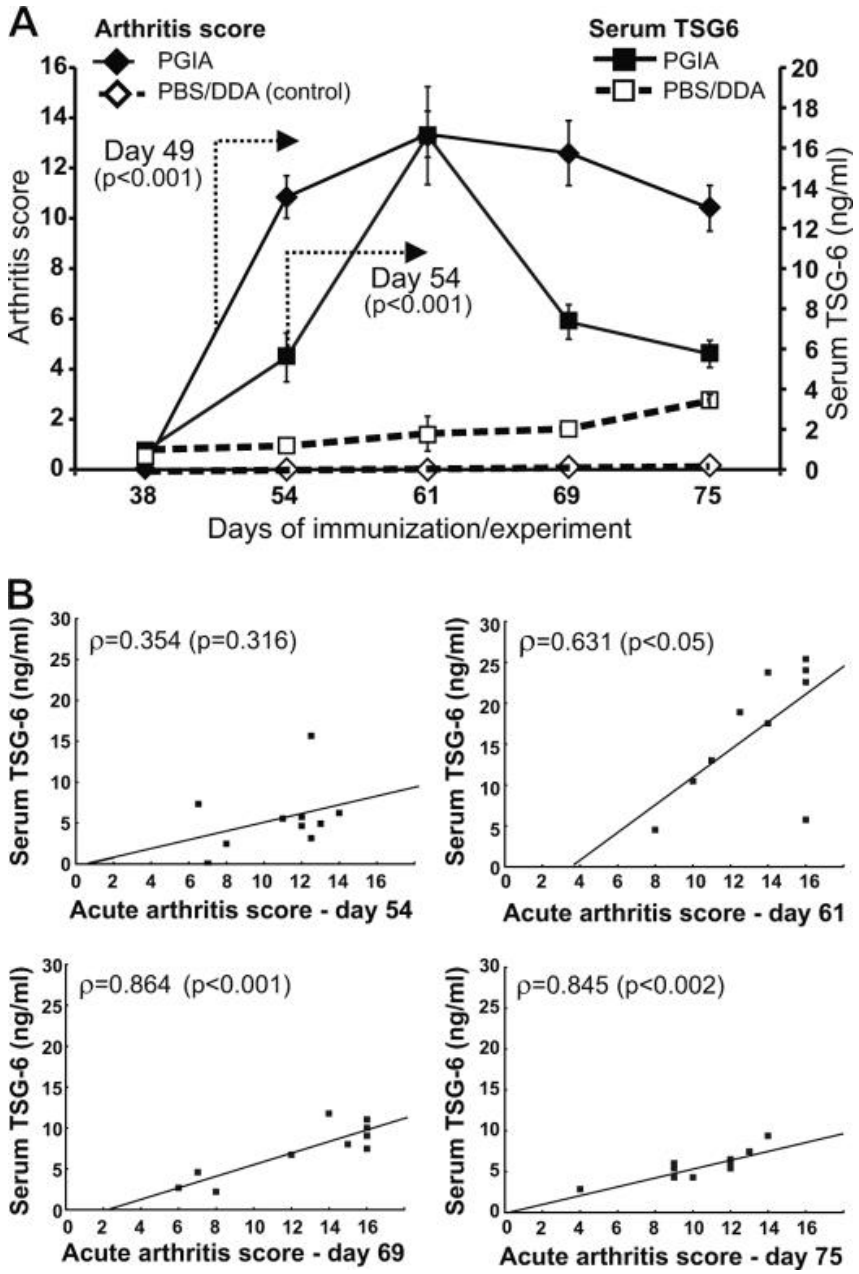

FIGURE 6.Correlation between arthritis severity and serum TSG-6 levels at different time points during the development of PGIA.

A, mice immunized with human cartilage PG in DDA adjuvant were scored for arthritis severity twice a week after the second immunization (Day 21), and serum was collected weekly up to day 75 after the first immunization. Control groups were injected with PBS/DDA emulsion. Arthritis scores on the left Y axis, and serum TSG-6 concentrations on the *right y axis* are shown at five selected time points of immunization. Data shown are the mean ± S.E. (*error bars*) (n = 10 mice/group/time point). Statistically significant differences (p < 0.001) between the PGIA and PBS/DDA-injected groups from the indicated time point are depicted with *arrows*. Data were analyzed using repeated measures analysis of variance.

B, correlations between serum TSG-6 levels are indicated by Spearman's ρ values and corresponding p values at four different time points after the first PG/DDA immunization.

Table III. **Serum TSG-6 and cytokine concentrations and their correlation with arthritis and/or serum TSG-6 levels at selected time points in PGIA**

		Day 38	Day 54	Day 61	Day 69	Day 75
TSG-6		0.0	5.59 ± 1.31	16.6 ± 2.45	7.34 ± 1.06	5.77 ± 0.57
	Arthritis	(*NS*)	(*NS*)	(*0.631/0.050*)	(*0.864/0.001*)	(*0.845/0.002*)
IL-6		6.68 ± 0.68	17.5 ± 1.57	19.18 ± 3.29	14.30 ± 0.85	15.65 ± 1.01
	TSG-6	(*NS*)	(*NS*)	(*0.760/0.017*)	(*NS*)	(*NS*)
	Arthritis	(*NS*)	(*NS*)	(*0.720/0.029*)	(*NS*)	(*NS*)
IL-17		0.61 ± 0.39	5.27 ± 0.74	7.54 ± 1.30	5.35 ± 0.47	4.81 ± 0.20
	TSG-6	(*NS*)	(*NS*)	(*0.894/0.007*)	(*NS*)	(*NS*)
	Arthritis	(*NS*)	(*NS*)	(*0.935/0.002*)	(*NS*)	(*NS*)
TNF-α		1.38 ± 0.51	9.27 ± 0.77	9.28 ± 0.39	8.34 ± 1.14	8.25 ± 0.31
	TSG-6	(*NS*)	(*NS*)	(*NS*)	(*0.841/0.018*)	(*NS*)
	Arthritis	(*NS*)	(*NS*)	(*NS*)	(*0.741/0.057*)	(*NS*)
IL-1β		7.40 ± 0.92	9.50 ± 1.23	9.20 ± 1.20	9.31 ± 0.96	7.85 ± 0.89
	TSG-6	(*NS*)	(*NS*)	(*NS*)	(*NS*)	(*NS*)
	Arthritis	(*NS*)	(*NS*)	(*NS*)	(*NS*)	(*NS*)

Table III. The numbers in the first rows indicate mean ± S.E. of TSG-6 or cytokine concentrations (pg/ml) in serum at five selected time points (days 38, 54, 61, 69, and 75 after the first PG immunization) (n = 10 mice). Numbers in parentheses in italic type (Spearman's correlation coefficient/corresponding p value) in the second and third rows depict significant correlation with serum TSG-6 levels and arthritis score, respectively. *NS*, correlation is not significant.

Whereas serum TSG-6 concentrations showed a strong positive correlation with arthritis severity from day 61 to 75 after the first immunization (Fig. 6A and Table 3), serum levels of other "arthritis signature" pro-inflammatory cytokines (such as IL-6, IL-17, and TNF-α) correlated with the arthritis scores and serum TSG-6 at the acute or subacute phase (day 61 or 69) of PGIA, whereas serum IL-1β concentrations increased in response to immunization and subsequent arthritis onset but did not seem to correlate with disease severity or serum TSG-6 (Table 3). No correlation between serum TSG-6 levels and the concentrations of anti-PG Abs in serum or the magnitude of PG-specific T-cell responses could be detected. (data not shown).

TSG-6 in synovial fluid and tissue extracts of inflamed joints of mice with PGIA

As illustrated in the *histology panel* in Fig. 7A), the involved paws were heavily infiltrated by inflammatory cells and also showed histological evidence of cartilage and bone destruction at an advanced stage of acute arthritis (61 days after the first immunization). At this stage of PGIA, we harvested synovial fluid from arthritic ankle joints and prepared tissue extracts from the inflamed paws for measurement of TSG-6 content by ELISA and Western blotting. The amount of TSG-6 in pooled samples of synovial fluid was 110 ± 7 pg/mg protein, and it ranged from 20 to 550 pg/mg protein in the extracts of inflamed paws and from 0 to 60 pg/mg protein in non-arthritic control paws, as determined by ELISA. Western blotting demonstrated the presence of TSG-6 in both synovial fluid and tissue samples (Fig. 8A). In both cases, TSG-6 was found mostly in the form of high molecular weight complexes (most likely composed of TSG-6 and a heavy chain (HC1 and/or HC2) of IαI (61,62)); only small amounts of the free form could be detected (Fig. 8A).

Interestingly, synovial fluid contained a single TSG-6-positive band at ~120–125 kDa, whereas the extracts of inflamed paws showed multiple bands below that size (Fig. 8A, *lanes 1* and *2*). A Western blot of paw extracts revealed two TSG-6 bands at ~125 and ~80 kDa, respectively (Fig. 8A). Both of these bands were also recognized by an anti-mouse HC1 Ab, but only the upper band was recognized by anti-HC2 Ab (Fig. 8A).

Figure 7.

Figure 7. Histology of the inflamed paw on day 61 of PGIA and localization of TSG-6 in inflamed tissue and mast cells. (***A***) the entire ankle-paw region of an arthritic hind limb is shown in a low magnification montage picture. The section was stained with H&E. The *arrows* show the areas of cartilage and bone destruction by inflammatory synovium, and the area from which synovial fluid was harvested is also indicated.

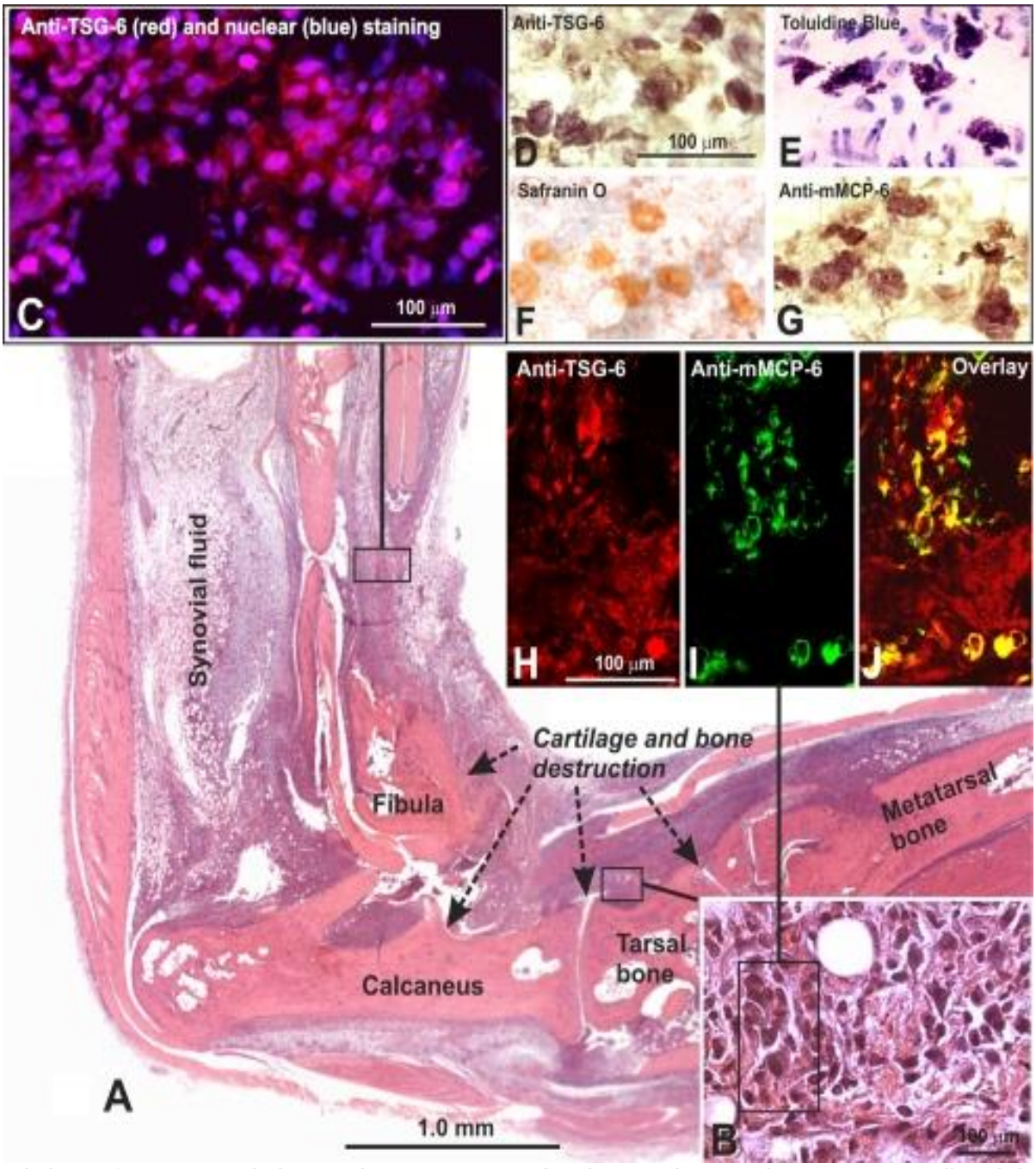

(***B***) A high magnification insert at the *bottom right corner* represents inflamed periarticular tissue where TSG-6-positive cells (including mast cells) were found in frozen sections of hind limbs with similar arthritis scores.
(*C*) immunostaining of inflamed tissue with anti-TSG-6 mAbs (*red fluorescence*) identified several TSG-6-expressing cells (nuclei were stained *blue with DAPI*).
(D) Mast cells, which showed strong and distinct immunostaining for TSG-6 in their secretory granules, were identified by toluidine blue **(*E*)** safranin O **(*F*)** and anti-mouse mast cell protease **(*G*)** (mMCP-6; mast cell tryptase) staining. In areas similar to that framed in *B* TSG-6 (*red*) **(*H*)** and mMCP-6 (*green*) **(*I*)** co-localized in mast cells as shown in the *overlaid image* (*yellow*) **(*J*)**.

Figure 8.

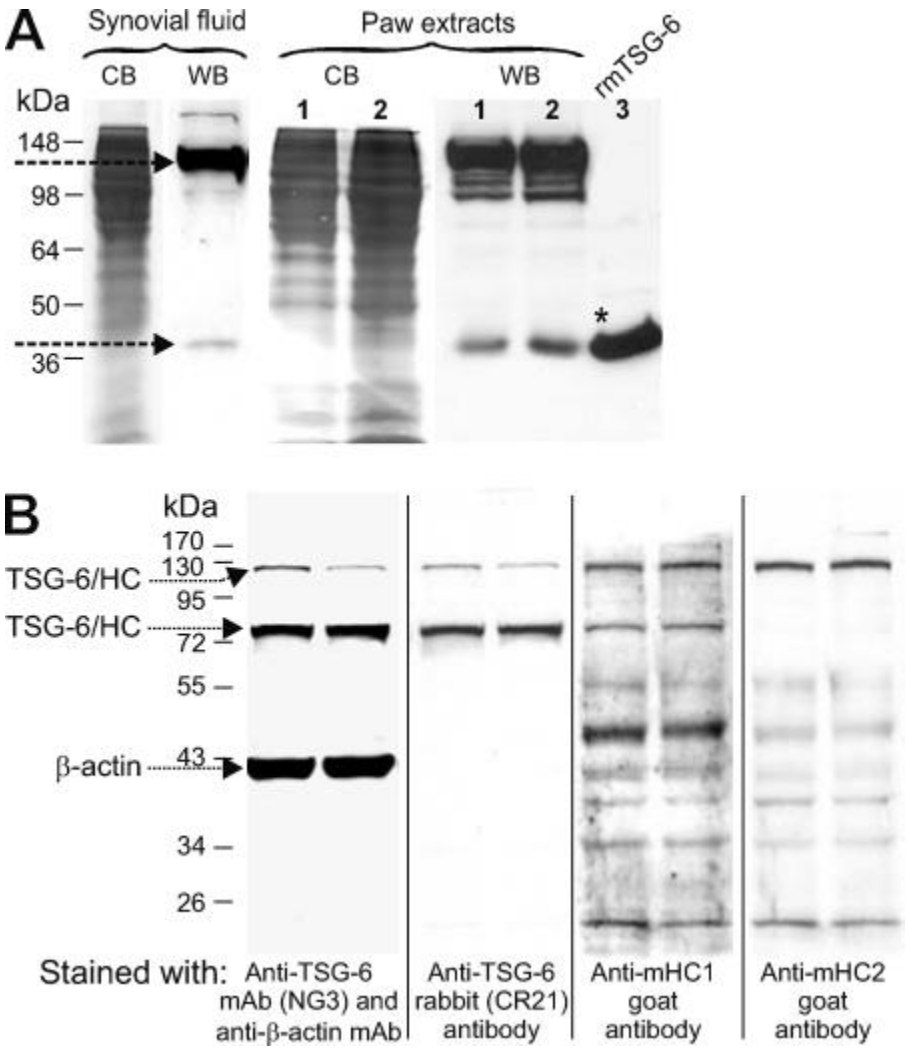

Figure 8:Western blot analysis of TSG-6 in synovial fluid and in tissue extracts of inflamed paws of mice with PGIA. (*A*) The Coomassie Blue (*CB*)-stained strips represent total protein from synovial fluid (*first lane*) or tissue extracts of arthritic paws (*first* and*second lanes* in the *left panel* under *Paw extracts*), harvested on the peak of arthritis (day 61). Pooled synovial fluids (50 μl) after digestion with *Streptomyces* hyaluronidase or from 2 mg (*lane 1*) and 4 mg (*lane 2*) of protein of paw extracts from arthritic mice were separated by 12% SDS-PAGE. *Lane 3* contains 1 μg of purified rmTSG-6 protein (*) (without Fc2a tail). TSG-6 was detected with biotinylated RC21 antibody. The *arrows* point to the high molecular mass (~120-kDa) TSG-6 complex and free (~39-kDa) TSG-6

(*B*) Western blot analysis of TSG-6 and the heavy chains (HC1 and HC2) of IαI in tissue extracts of inflamed paws. Tissue extracts from two arthritic paws were loaded on 12% SDS-PAGE (20 μg of protein/lane). The proteins were transferred onto a nitrocellulose membrane, probed with mAbs to TSG-6 and β-actin, and then stripped and sequentially reprobed with RC21 anti-TSG-6 antibody, anti-HC1, and anti-HC2 antibody, respectively. The *arrows* point to the TSG-6-containing complexes (no free TSG-6 was detected in this case) and to β-actin (loading control). *WB*, Western blot.

Cellular localization of TSG-6 in the inflamed paws of mice with PGIA

TSG-6 could be detected in most of the cells of the inflamed tissue (Fig. 7, *C* and *H*), by using immunohistochemistry on frozen sections of arthritic hind limbs (similar to that shown in Fig. 7, *A* and *B*). Unexpectedly, the strongest immunostaining appeared to be localized within large, granulated cells (Fig. 7D). Such cells also showed metachromatic staining with toluidine blue (Fig. 7D) and red staining with safranin O (Fig. 7D), indicating that they could be connective tissue mast cells.

Antibody against the mast cell-restricted tryptase mMCP-6 for immunostaining of tissue sections was used to confirm the identity of this cell type. Anti-TSG-6 (Fig. 7H) and anti-mMCP-6 (Fig. 7, *G* and *I*) Abs both stained the same type of cell. Co-localization of TSG-6 (Fig. 7H , *red*) and mMCP-6 (Fig. 7J , *green*) was further confirmed by the overlay of images (Fig. 7J ,*yellow*) of sections simultaneously stained with fluorescent Abs against the respective molecules.

HA is a stronger competitor than heparin for TSG-6 binding

RmTSG-6 bound to either HA- or heparin-coated plates, although the amount of TSG-6 bound to heparin appeared to be less than the amount that bound to HA. This difference might be due to the different molecular mass of HA *versus* heparin or different affinity of TSG-6 with HA or heparin (54).

Although TSG-6 binding sites to HA and heparin are different (63,64), and an octasaccharide of HA is sufficient to bind TSG-6, these two GAGs may compete for and/or interfere with TSG-6 binding either in vivo or in vitro (54, 55) .

In a competitive inhibition assay, we compared how HA or heparin could compete for TSG-6 binding (Fig. 9). Indeed, whereas the *in vitro* preformed TSG-6·heparin complex could not inhibit TSG-6 binding to HA, the *in vitro* preformed TSG-6·HA complex inhibited TSG-6 binding to heparin. The controls confirmed that the TSG-6·HA complex can inhibit binding to HA, and the TSG-6·heparin complex can inhibit the TSG-6 binding to heparin (Fig. 9).

Figure 9.

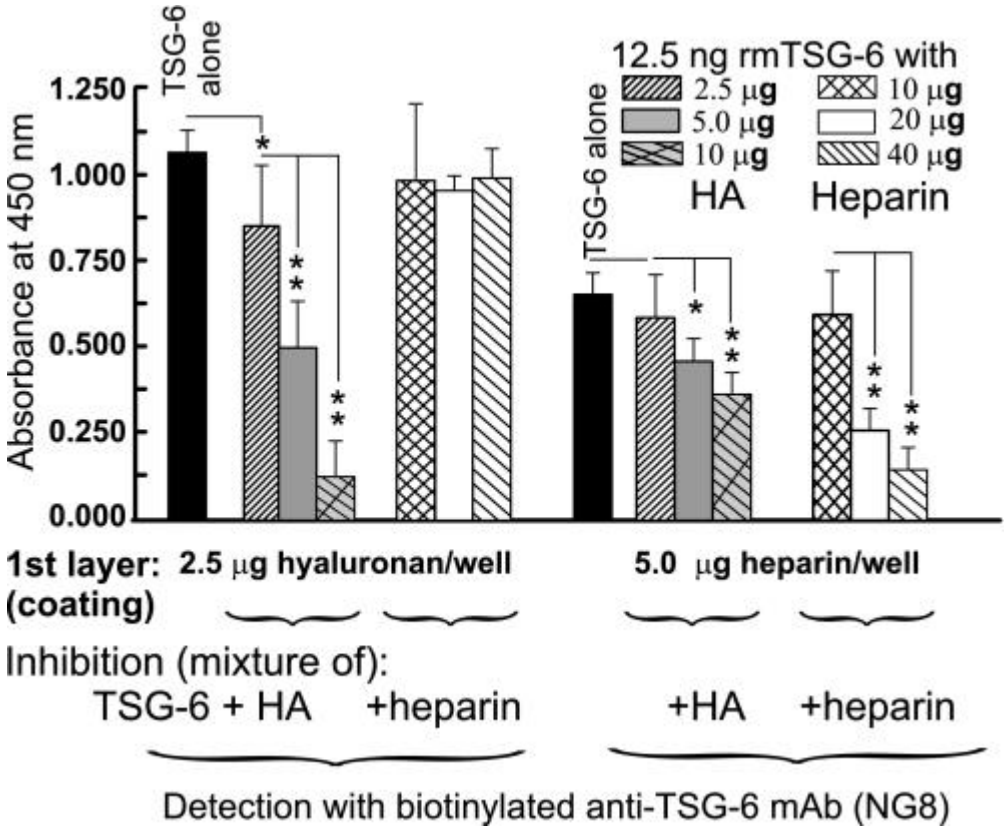

Competitive inhibition assay of TSG-6 binding to HA and heparin.

FIGURE 9. Competitive inhibition assay of TSG-6 binding to HA and heparin.
The optimal range of TSG-6 binding to HA- or heparin-coated plates was determined and then a competitive inhibition assay was performed. Three different concentrations were used for coating (2.5, 5, and 10 µg of HA or 5.0, 10, and 20 µg of heparin), and four different concentrations of TSG-6 in duplicate wells were assayed simultaneously in two plates. TSG-6 alone (50 ng in 100 µl of 0.5% BSA/PBS, *closed columns*), or the same amounts of TSG-6 were preincubated with HA or heparin (amounts of these GAGs are indicated) for 2 h at 37 °C prior to transferring to either HA- or heparin-coated wells.
TSG-6-binding was detected with biotinylated mAb NG8, and the reaction was developed with TMB substrate. Heparin only slightly inhibited or did not inhibit the binding of TSG-6 to HA, whereas HA could significantly inhibit TSG-6 binding to heparin (in a concentration-dependent manner). Significant differences are indicated with *asterisks* (*, $p < 0.05$; **, $p < 0.01$). *Error bars*, S.E.

TSG-6 binds mast cell tryptases in the presence of heparin or HA

Co-localization of TSG-6 and mMCP-6 in mast cells in inflamed joint tissue suggested that TSG-6 might be stored in mast cell granules, which are known to contain tryptases (mMCP-6 and mMCP-7 and heparin (56-58). Among other constituents, TSG-6 has been shown to bind either HA or heparin (54, 59, 60). In addition, TSG-6 can form a ternary complex with IαI in the presence of HA or heparin (54, 61). Then, it was of interest to determine whether TSG-6 could interact with mast cell tryptases in a similar manner *in vitro*. RmTSG-6, prebound to HA, could bind rmMCP-6 or (to a lesser extent) rmMCP-7, but this was not the case with TSG-6 prebound to heparin (Fig. 10A). In a reciprocal system, rmMCP-6 and rmMCP-7, bound to either HA or heparin, could bind TSG-6 (Fig. 10B).

Figure 10.

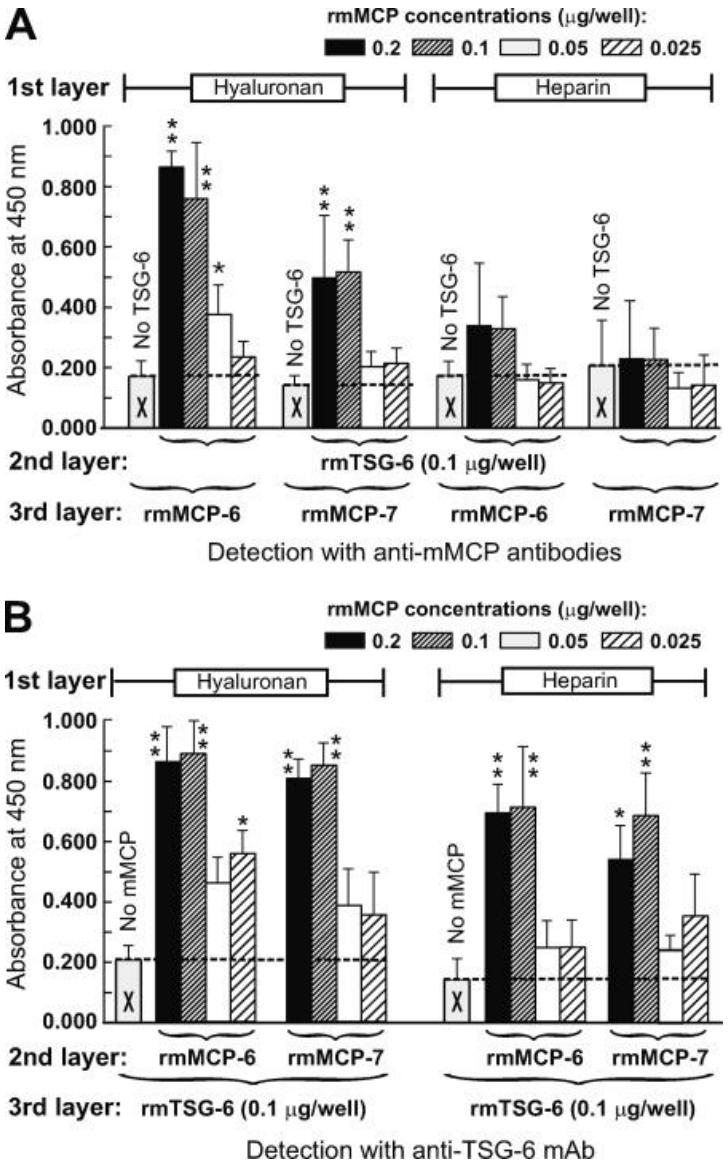

FIGURE 10. ***Measurement of the association of rmTSG-6 with mast cell tryptases (rmMCP-6 or rmMCP-7) and HA or heparin*** **in vitro.** The relative amounts of bound rmMCP-6 or rmMCP-7 after incubation of 0.1 μg of rmTSG-6/well with immobilized HA or heparin and the subsequent addition of various amounts of rmMCPs (concentrations are indicated at the *top*) can be seen on the graphs ***(A)***The relative amounts of bound rmTSG-6 after incubation of rmMCP-6 or rmMCP-7 (at concentrations indicated at the *top*) with HA or heparin and the subsequent addition of rmTSG-6 (0.1 μg/well) (*B*).Immobilization of HA and heparin and subsequent binding and detection of complexes formed between rmTSG-6 and rmMCP-6 or between rmTSG-6 and rmMCP-7 are described in detail under "Experimental Procedures." Base-line values (absorbance values resulting from direct binding of either TSG-6 or mMCPs to either HA or heparin) are indicated with *empty columns* with an X, and the base-line levels are indicated with *horizontal broken lines*. Mean ± S.E. values (*error bars*) of duplicate samples of three independent experiments are shown. Significant differences are indicated with *asterisks* (*, $p < 0.05$; **, $p < 0.01$).

TSG-6 can be co-immunoprecipitated with mast cell tryptases from tissue extracts of arthritic joints

TSG-6, mMCP-6, and mMCP-7 could be detected in relatively high amounts in tissue extracts of inflamed paws but were detected in lower amounts in tissue extracts of non-inflamed paws (Fig. 11, *A*–*C*). TSG-6 could be co-immunoprecipitated with both tryptases (especially with mMCP-6) (Fig. 11, *D*–*F*), which can suggest that complex formation between TSG-6 and mast cell tryptases (most likely via HA or heparin binding in secretory granules) did occur *in vivo* under inflammatory conditions.

Figure 11.

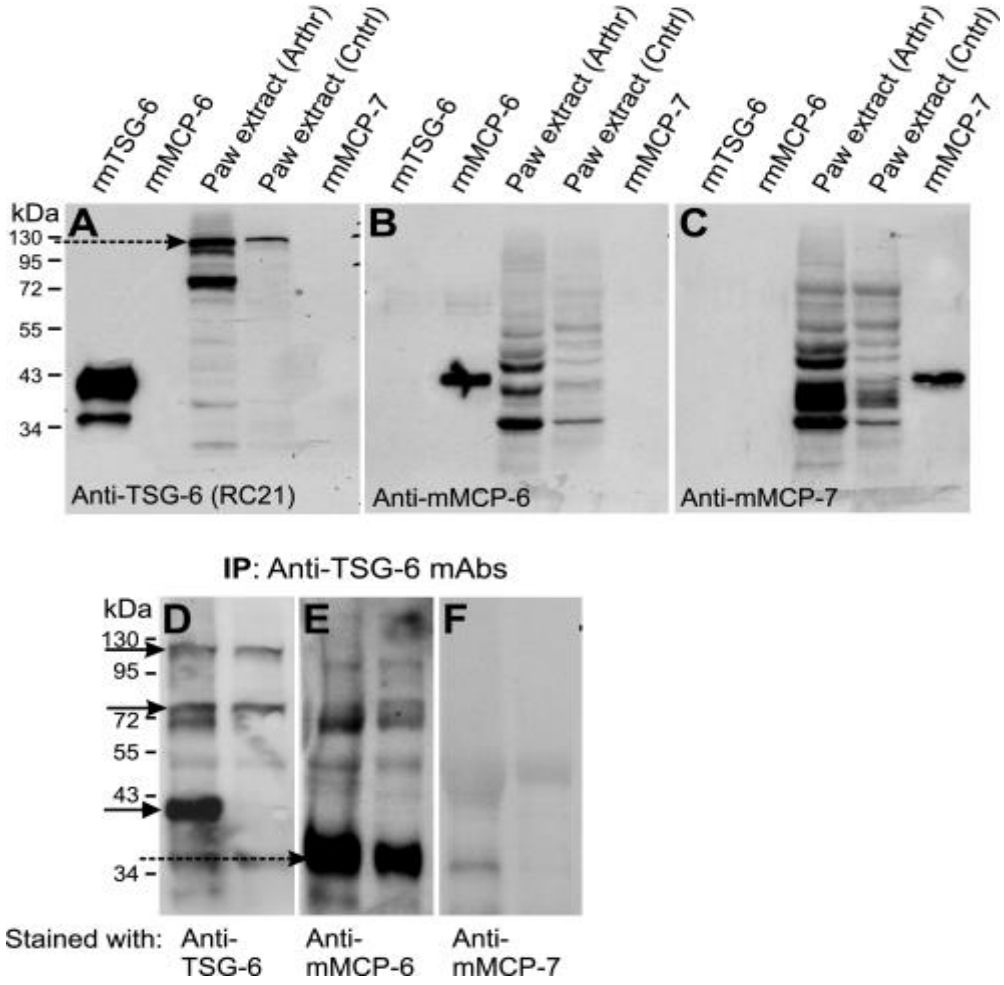

FIGURE 11. Western blots of TSG-6 and mast cell tryptases in arthritic and normal paw extracts and co-immunoprecipitation of *in vivo* formed TSG-6-tryptase complexes.

A–C, Western blots show the same membrane, which was stained with an antibody to TSG-6 (*A*) and then stripped and restained with antibodies to mMCP-6 (*B*) and mMCP-7 (*C*), respectively. The *lanes* were loaded with samples as follows: 0.2 μg of purified rmTSG-6, 0.1 μg of recombinant mMCP-6, tissue extract (50 μg of protein) from arthritic mouse paw (*Arthr*), extract (50 μg of protein) from normal control paw (*Cntrl*), and 0.05 μg of mMCP-7. *D–F*, extracts of arthritic (*left lanes*) or normal (*right lanes*) mouse paws were immunoprecipitated (*IP*) with a mixture of anti-TSG-6 mAbs (as described under "Experimental Procedures") and then blotted (*WB*) with anti-TSG-6 (RC21) (*D*), anti-mMCP-6 (*E*), and anti-mMCP-7 antibodies (*F*). The*arrows* point to the highest and lowest molecular weight TSG-6 species in *D*. The *broken arrow* indicates the TSG-6 coimmunoprecipitatedmMCPs.

TSG-6 (also called TNFAIP6) is a hyaluronan (HA)-binding protein, secreted by a variety of cells in response to proinflammatory stimuli (60, 61). TSG-6 protein has been detected in large quantities in the synovial fluids and synovial tissues of inflamed joints of patients with rheumatoid arthritis (22, 23). Recombinant mouse TSG-6 (rmTSG-6) has demonstrated anti-inflammatory and chondroprotective effects in mouse models of rheumatoid arthritis (31). TSG-6 forms a stable complex with a heavy chain (HC) of inter-α-trypsin inhibitor (IαI), a major serine protease inhibitor in serum (62). Because IαI exhibits increased inhibitory activity against plasmin, a key activator of matrix metalloproteinases after encountering TSG-6, it has been postulated that TSG-6 exerts its anti-inflammatory and chondroprotective effects primarily through inhibition of the protease network (32, 44).

TSG-6 consists of a "Link" module and a "CUB" (complement C1s/C1r-, uEGF-, BMP-1-like) domain. The positively charged Link module binds various glycosaminoglycans (GAGs), including HA, chondroitin sulfate, heparin, and heparan sulfate (54, 59, 60). The CUB domain of TSG-6 is similar to the CUB module found in several developmentally regulated proteins that are thought to be involved in protein-protein interactions (25-27). However, to date, only fibronectin has been shown to bind to the CUB domain of TSG-6 (39). TSG-6 is not expressed constitutively but can be induced by proinflammatory cytokines or LPS (22, 31, 40). In contrast, anti-inflammatory cytokines, such as IL-4 or IL-10, suppress TSG-6 expression either directly or via inhibition of LPS/Toll-like receptor-induced cell activation (40).

TSG-6 can modulate the binding of HA to the cell surface HA receptor, CD44 (35). Treatment of leukocytes with soluble HA·TSG-6 complex has been shown to inhibit the CD44-mediated adhesion of these cells to immobilized HA *in vitro* (33). Because the CD44-supported adhesion (rolling) of leukocytes on HA-covered surfaces of inflamed vascular endothelium is required for the emigration of these cells from the bloodstream into inflamed tissue, inhibition of this adhesion step by the HA·TSG-6 complex could have a negative impact on the extravasation of inflammatory cells (36).

The *in vitro* observations are consistent with *in vivo* studies reporting reduced leukocyte influx into the arthritic joints of TSG-6-treated mice and enhanced leukocyte extravasation in the joints of TSG-6-deficient mice (31, 32, 34). Collectively, the *in vivo* observations lend

support to the concept that TSG-6 has a critical role in the resolution of inflammation, but this function of TSG-6 may rely on more than one mechanism.

One of the initial goals of the present study was to develop a sensitive detection method for measuring the concentrations of TSG-6 in serum and synovial fluid samples of mice with arthritis. Using cartilage proteoglycan (PG)-induced arthritis (PGIA) in BALB/c mice, we monitored serum levels of TSG-6 in correlation with the onset and progression of arthritis and identified TSG-6-positive cells in the joints. Although many connective tissue cells were TSG-6-positive in the arthritic joints, unexpectedly, the strongest immunostaining of TSG-6 was detected in the granules of mast cells that accumulated in inflamed paws of mice. *In vitro*, rmTSG-6 bound to both heparin and the mast cell-restricted tryptases, murine mast cell protease-6 (mMCP-6) and mMCP-7, two major serine proteases present in mast cell secretory granules (56). Further, TSG-6 could be co-immunoprecipitated with both mMCP-6 and mMCP-7 from tissue extracts of arthritic paws, in which the heavy chains (HC1 and HC2) of IαI were also present. These data suggest that TSG-6 may modulate mast cell function via its interactions with key components of secretory granules.

Discussion

In some studies, up to 72% of patients who are diagnosed with RA have been shown to have TMJ pathology as a result of the disease (63). This number is similar in longstanding RA and in patients with juvenile idiopathic arthritis (38, 52, 63-65). Analysis of synovial fluid samples from the TMJ of symptomatic patients with RA or OA have been shown to demonstrate the involvement of this joint in both diseases (16, 63, 64). The TMJ can also become a target in animal models of the human disease, therefore it was quite surprising that the involvement of TMJ in PGIA has not been investigated, and to our knowledge, to date this is the first time it has been done. We were also first to describe that in PGIA, the TMJ involvement resembles OA rather than RA as the cartilage of the affected mice resembled more the degenerative changes described in humans and in other animal models of OA (50, 66). In other affected joints like the ankle there is usually severe synovitis and loss of chondrocytes from the superficial zones of the cartilate (pitting). The latter is more characteristic to sites where the cartilage in the proximity of inflammatory cells. Aggreccan degradation and the loss of aggreccan fragments can be observed in these joints in the entire cartilage. In the TMJ the aggreccan degradation is to a similar extent and less progressive that in the other observed joints. In animals with acute or chronic PGIA and obvious inflammatory arthritis in the limbs, the predominant picture seen employing histological techniques is the degenerative changes in the mandibular cartilage with the agreccan loss only occasionally associated with structural damage like fibrillation and fissures. This implies that in the TMJ, the loss of aggrecan is the result of a different stimulus and different immune response compared to those in the affected limbs. The above histological observations were not present in the control animals treated with PBS or DDA. This excluded the possibility of any ago- or gender related association (67).

Catabolic enzymes responsible for fragmentation of aggrecan thought to be aggrecanases (ADAMTS-4 and ADAMTS-5) (68, 69) and stromelysin (MMP-3) (9, 70-74). We found high mRNA levels of these enzymes and neoepitopes produced by these enzymes (-NITEGE and –VDIPEN) in the TMJs of diseased animals similarly to other affected joints. Pro-inflammatory cytokines responsible for upregulation of these enzymes include IL-1β (75) directly and indirectly TNF-α and IL-6 through IL-1β pathway (50, 51). IL-1β has also been shown to be produced in response to various stimuli by the chondrocytes in the cartilage which in time

leads to local destruction of pericellular matrix (50). Transgen mice expressing chondrocyte-specific IL-1β gene develop OA-like histopathological changes in the TMJs. It has also been shown that there is a connection between serum levels of IL-1 receptor and the presence of arthritis in the TMJ in patients with RA (50). In our model, although IL-1β was not upregulated in the mandibular cartilage but it was significantly up-regulated in other joints of diseased animals which lead to increased serum levels in these animals. Serum samples from arthritis mice showed high concentration of IL-1β and other pro-inflammatory cytokines like TNFα, IL-6 and IL-17 similarly to concentrations found in synovial fluid of the TMJ of RA and OA patients (64, 76, 77). This, we thought, was ultimately responsible for OA the like picture of cartilage degeneration in the mandibular cartilage. Our investigations suggest that the TMJ not affected by the autoimmune inflammation characteristic for the disease in other joints in PGIA. Increased cytokine levels in the serum as a result of higher production in affected inflamed joints results in an OA-like picture in the TMJ. The chronic production of these pro-inflammatory cytokines lead to TMJ cartilage degradation over time. As serum concentrations of pro-inflammatory cytokines diminish as the disease progresses in late phase of chronic PGIA (19, 20) further investigations might show a slowing down of TMJ cartilage degradation over time.

In conclusion, we demonstrated that the TMJ is not affected by autoimmune arthritis in mice with PGIA. The cartilage matrix degradation seen in these joints is likely to be the result of a systemic overproduction of pro-inflammatory cytokines. Therefore early treatment of RA targeting these cytokines may hold promise to prevent irreversible tissue damage in the TMJs of affected patients with RA (64, 78, 79).

Mast cells are part of the native immune system and have a paramount role in parasite and helminth infections and are involved in various IgE mediated allergic reactions. A high number of these cells can be found usually around blood vessels where they have access to IgEs and IgGs from both the circulation and the tissues (80). Upon activation, mast cells release their secretory granules containing proteases such as mMCP-6 and 7 (murine orthologs of human β-tryptases) (81), GAGs and proinflammatory cytokines into the extracellular matrix (56). These proteases are found in complexes with serglycin PGs

through electrostatic interactions between their positively charged amino acid residues and the negatively charged GAG (heparin or chondroitin sulfate E) side chains of serglycin. Heparin is thought to have a role in maintenance of tryptases in an active conformation at low pH inside the mast cell granules. When the tryptase-heparin complex containing granules are released, the neutral pH of the ECM increases the proteolytic activity (57, 81). There have been increasing number of reports about the role of mast cells in non-IgE mediated diseases such as arthritis. A large number of mast cells has been shown to be present in the inflamed arthritic joints of both mice and humans (82, 83). Tryptases found in mast cell activate MMP-3 (9, 70-74), which then activates synoviocyte procollagenase and also cleaves cartilage aggrecan (84). Mast cell KO mice (*W/W^v* mutant) are less susceptible to inflammatory arthritis when compared with wild types (85). mMCP-6 and 7 deficient mice and KO mice lacking enzymes necessary for heparin synthesis exibit reduced joint cartilage degradation in arthritis (86). mMCP-6 heparin complexes are also known to stimulate neutrophil extravasation via induction of chemokines (87). This influx of neutrophils into the joints is a well known phenomenon of both human and animal models of arthritis (85, 88).

The protective role of TSG-6 has been shown in various animal models of RA. TSG-6 deficient mice develop more severe arthritis after immunization with cartilage PG when compared to wild type counterparts (27, 34, 44). TSG-6 gene has been described as a marker for early inflammatory events in other immune diseases (31, 38, 53) and in PGIA, TSG-6 gene expression can be demonstrated in the synovial tissue well before the clinical symptoms of arthritis develop. The kinetics of TSH-6 production during the progression of autoimmune diseases are yet to be investigated. In our prior studies, animals injected intra articularly with rmTSG-6 and other animals expressing TSG-6 transgene in cartilage exhibited substantial chondroprotective effects in murine models of arthritis (31, 44). Systemic administration of IV rmTSG-6 into mice with PGIA was shown to reduce the presence of leukocytes in the joints (31). TSG-6 was also found to reduce influx of neutrophyos into zymosan-stimulated air pouches as a result of decreased chemokine concentration at the site of inflammation (89). On the contrary, increased recruitment of neutrophils into the joints and peritoneal cavity after peritonitis induction has been observed in TSG-6 deficient mice

(34). These investigations support the role of TSG-6 in the down regulation of the activity of matrix-degrading proteases likely including mast cell triptases (31, 44).

TSG-6 readily forms a covalent complex with the HC1 or HC2 subunit of the serine protease inhibitor IαI (composed of two HCs bound to the chondroitin sulfate chain on bikunin, a Kunitz type protease inhibitor) and augments the inhibitory capacity of this molecule (19). Recent studies indicate that potentiation of IαI activity is achieved by the TSG-6-mediated transfer of a HC from the single chondroitin sulfate side chain of bikunin onto HA (90, 91). This is followed by the release of bikunin with a single HC (*i.e.* pre-IαI) or without HC (although release of free bikunin has not been observed *in vitro*). Bikunin, which harbors the protease-inhibitory activity of IαI, is more active in the absence than in the presence of the HCs on its GAG chain (54). Intriguingly, the tryptase inhibitor (designated "trypstatin") present in mast cells has been identified as bikunin. Because only bikunin protein but not mRNA could be detected in mast cells, the authors concluded that bikunin was trapped by these cells from serum of circulating blood (92, 93). It is tempting to speculate that TSG-6 has a role in liberating bikunin from IαI and trapping it inside the mast cell granules or on the surface of granule membranes. Upon mast cell exocytosis (*i.e.* the inflammation-induced release of granule contents into the extracellular space), the tryptases would meet bikunin and thus be inactivated.

In our study, as a first step of generating a highly sensitive assay, we constructed an expression vector that contained both TSG-6 and mouse IgG2a-Fc fusion partner cDNA, separated by an endoprotease cleavage site (Ile-Glu-Gly-Arg) specific for factor Xa (which converts prothrombin to thrombin). We also developed a stepwise cloning procedure for rapid selection of CHO transfectants with the highest yield of rmTSG-6 fusion protein released into serum-free medium. RmTSG-6 protein was then used to generate B cell hybridomas from TSG-6-deficient mice and to select pairs of mAbs for capture ELISAs, where rmTSG-6 could also be employed as a reference standard. Some of the anti-TSG-6 mAbs were also suitable for immunoprecipitation, Western blotting, and immunohistochemistry. We then immunized BALB/c mice with cartilage PG to induce PGIA. Our aims were to compare the kinetics of serum TSG-6 levels with the severity of arthritis and other disease markers and to determine whether it accumulates at the sites of inflammation (34). We were able to measure TSG-6 levels in synovial fluid and tissue extract speciments of paws of mice in the

acute phase of inflammation. Serum TSG-6 concentrations showed a more significant positive correlation with the advancement of arthritis (Fig. 6) than other pro-inflammatory cytokines known to have association with arthritis like IL-6, IL-17, TNF-α and IL-1β. These cytokines although showed some correlation with the disease development but only at certain time points (Table 3). The late or chronic phase of PGIA is associated with tissue destruction followed by synovial fibrosis and bone remodeling (Fig. 7) (19, 34). During this phase serum TSG-6 levels steadily declined (Fig. 6). Our Western blot analysis showed that the majority of TSG-6 was present as a high molecular weight species (Fig. 8) indicating that at these inflammatory sites, TSG-6 was probably complexed with HCs from IαI, as described before (19, 44). The inflammatory paw extracts consistently contained both a ~125-kDa species (probably a TSG-6·HC1 and a TSG-6·HC2 complex) (Figs.8 and 11) and an ~80-kDa species (Figs.8B). The latter band could be a degradation product of the TSG-6·HC1 complex and was not detected in synovial fluids of arthritic joints.

Employing immunohistochemistry on the acutely inflamed joints of mice with our newly generated mAbs, we found that although most cells in the arthritic joint contain low to moderate concentration of TSG-6, high concentration was present in the secretory granules of activated mast cells with most of these cells showing signs of degranulation into the inflamed tissues (Fig. 7). The identity of these cells were confirmed using metachromatic, safranin O and Abs to mouse mast cell-specific protein. To confirm the localization of TSG-6 in the granules of mast cells we employed an Ab against the mast cell specific tryptase mMCP-6, which is known to be present in the secretory granules, along with Abs against TSG-6. The overlapping signals of these two antibodies confirmed the colocalisation of these two proteins in the mast cells (Fig. 7). Since both mMCP-6 and TSG-6 can bind heparin, we sought to find out whether these two proteins could connect via heparin (54, 57, 58). Indeed, our *in vitro* studies revealed a tripartite association of rmTSG-6 with rmMCP-6 (and, to a lesser extent, with rmMCP-7) through heparin as well as through HA (Fig. 10). Both MMCP-6 and 7 could be pulled down by TSG-6 immunoprecipitates of arthritic paw extracts (Fig. 11) indicating that their function is connected in vivo during joint inflammatory conditions.

This is the first time that TSG-6 has been demonstrated in mast cells. We have also shown that mMCP-6 and mMCP-7 are associated with TSG-6 after binding to either HA or heparin. TSG-6 coupled with HA makes a stonger bond with both tryptases than coupled with heparin

(Fig. 10). This could partly be explained that Has better absorption to plastic surfaces with high molecular mass HA (1,000–2,000 kDa) than low molecular heparin. Nonetheless, in a competitive inhibitoion assay HA inhibited the binding of rmTSG-6 to heparin, but it was not true vice versa (Fig. 9). In any case, our in vitro assays clearly demonstrated the enhancement of TSG-6 tryptase interactions on the GAG-coated surfaces (Fig. 10). Co-immunprecipitation of TSG-6 and tryptases indicate that it is likely that complex formation also happens in vivo (Fig. 11).

Collectively, these data argue for a role of TSG-6 in the resolution of inflammation, in part due to a negative influence on mast cell protease-induced chemokine production and subsequent leukocyte extravasation. More extensive investigations are necessary to determine the type of molecular interactions among HA, heparin, TSG-6 and tryptases and to investigate whether or not TSG-6 plays a regulatory role in tryptase-bikunin interactions in mast cell granules. As a whole, the novel functions of TSG-6 in prevention of inflammatory joint destruction warrants further investigation.

Summary

In this present study, I was investigating the involvement of the TMJ in mice with PGIA and the role of TSG-6 in in mice with PGIA. My new findings are as follows:

- There are pathologic changes in the temporomandibular joint in mice with PGIA and these changes resemble OA rather than RA.
- I described a simple expression system for high yield production of functionally active rmTSG-6.
- Serum TSG-6 concentrations correlate with arthritis severity and serum levels of proinflammatory cytokines
- but not with immune responses in PGIA
- The strongest expression of TSG-6 is in mast cells in the inflamed tissues
- The likely role of TSG-6 is that it modulates mast cell function via its interactions with key components of secretory granules.

Összefoglalás

PhD értekezésemben a temporomandibuláris ízület érintettségét, illetve a TSG-6 szerepét vizsgáltam proteoglikán indukált artritiszes egerekben. Eredményeim:

- Vannak patológiás elváltozások proteoglikán indukált artritiszes egerek temporomandibuláris ízületében, azonban ezek inkább osteoarthritiszre mint rheumatoid artritiszre emlékeztetnek.
- Leírtam egy módszert az aktív mTSG-6 kimutatására
- A szérum TSG-6 koncentráció arányos az artritisz súlyosságával, de
- Az immunválasz mértékével nem
- A legnagyobb TSG-6 expresszió a gyulladt szövetekben a hízósejtekben figyelhető meg.
- A TSG-6 legvalószínűbb funkciója a hízósejtek funkciójának modulálása a szekréciós granulumok modulálásán keresztül

References

1. Roth C, Ward R, Tsai S, Zolotor W, Tello R. MR imaging of the TMJ. Applied Radiology
2. Zadik Y, Aktaş A, Drucker S, Nitzan D. Aneurysmal bone cyst of mandibular condyle: A case report and review of the literature. Journal of Cranio-Maxillofacial Surgery. 2012;40:243-8.
3. Okeson. 2003:233.
4. Tuz H, Onder E, Kisnisci R. Prevalence of otologic complaints in patients with temporomandibular disorder. American Journal of Orthodontics and Dentofacial Orthopedics 2003;123:620–3.
5. Ramírez LM SG, Ballesteros LE Temporomandibular disorders: referred cranio-cervico-facial clinic. Medicina oral, patologia oral y cirugia bucal. 2005:18–26.
6. Peroz. Otalgia and tinnitus in patients with craniomandibular dysfunctions. 2001:713–8.
7. Haskin C, Milam S, Cameron I. Pathogenesis of degenerative joint disease in the human temporomandibular joint. Critical Reviews in Oral Biology & Medicine. 1995;6:248–77.
8. Tanaka E, Detamore M, Mercuri L. Degenerative disorders of the temporomandibular joint: etiology, diagnosis, and treatment. Journal of Dental Research. 2008;87:296–307.
9. Ghassemi Nejad S, Kobezda T, Tar I, Szekanecz Z. Development of temporomandibular joint arthritis: The use of animal models. Joint Bone Spine. 2017;84(2):145-51.
10. Conaghan P. Osteoarthritis - National clinical guideline for care and management in adults. 2008.
11. Albani S, Carson D, Roudier J. Genetic and environmental factors in the immune pathogenesis of rheumatoid arthritis. Rheumatic Disease Clinics of North America. 1992;18:729–40.
12. Goronzy J, Weyand C. Developments in the scientific understanding of rheumatoid arthritis. Arthritis Research & Therapy 2009:249.
13. Franks A. Temporomandibular joint in adult rheumatoid arthritis. A comparative evaluation of 100 cases. Annals of the Rheumatic Diseases. 1969;28:139–45.
14. Gleissner C, Kaesser U, Dehne F, Bolten W, Willershausen B. Temporomandibular joint function in patients with longstanding rheumatoid arthritis - I. Role of periodontal status and prosthetic care - a clinical study. European Journal of Medical Research. 2003;8:98–108.
15. Ueno T, Kagawa T, Kanou M, Ishida N, Fujii T, Fukunaga J. Pathology of the temporomandibular joint of patients with rheumatoid arthritis--case reports of secondary amyloidosis and macrophage populations. Journal of Craniomaxillofacial Surgery. 2003;31:252–56.
16. Gynther G, Holmlund A, Reinholt F, Lindblad S. Temporomandibular joint involvement in generalized osteoarthritis and rheumatoid arthritis: a clinical, arthroscopic, histologic, and immunohistochemical study. International Journal of Oral & Maxillofacial Surgery 1997;26:10–6.
17. Harper R, Kerins C, McIntosh J, Spears R, Bellinger L. Modulation of the inflammatory response in the rat TMJ with increasing doses of complete Freund's adjuvant. Osteoarthritis Cartilage. 2001;9:619–24.
18. Habu M, Tominaga K, Sukedai M, Alstergren P, Ohkawara S, Kopp S. Immunohistochemical study of interleukin-1beta and interleukin-1 receptor antagonist in an antigen-induced arthritis of the rabbit temporomandibular joint. Journal of Oral Pathology & Medicine. 2002;31:45–54.

19. Glant T, Finnegan A, Mikecz K. Proteoglycan-induced arthritis: immune regulation, cellular mechanisms, and genetics. Critical Reviews in Immunology. 2003;2003:199-250.
20. Glant T, Mikecz K. Proteoglycan aggrecan-induced arthritis: a murine autoimmune model of rheumatoid arthritis. Methods in Molecular Medicine. 2004;102:313-38.
21. Lee T, Wisniewski H, Vilcek J. "A novel secretory tumor necrosis factor-inducible protein (TSG-6) is a member of the family of hyaluronate binding proteins, closely related to the adhesion receptor CD44. Journal of Cell Biology. 1992;116:545–57.
22. Wisniewski HG, Maier R, Lotz M, Lee S, Klampfer L, Lee TH, et al. TSG-6: a TNF-, IL-1-, and LPS-inducible secreted glycoprotein associated with arthritis. Journal of Immunology. 1993;151:6593–601.
23. Stanker LH, Vanderlaan M, Juarez-Salinas H. Journal of Immunological Methods. One-step purification of mouse monoclonal antibodies from ascites fluid by hydroxylapatite chromatography. 1985;76:157–69.
24. Wisniewski HG, Burgess WH, Oppenheim JD, Vilcek J. TSG-6, an arthritis-associated hyaluronan binding protein, forms a stable complex with the serum protein inter-alpha-inhibitor. Biochemistry Society Transactions. 1994;33:7423–9.
25. Bork P, Beckmann G. The CUB domain. A widespread module in developmentally regulated proteins. Journal of Molecular Biology. 1993;231:539–45.
26. Zhang P, Pan W, Rux AH, Sachais BS, Zheng XL. The cooperative activity between the carboxyl-terminal TSP1 repeats and the CUB domains of ADAMTS13 is crucial for recognition of von Willebrand factor under flow. Blood. 2007;110:1887–94.
27. Major B, Kardos J, Kékesi KA, Lorincz Z, Závodszky P, Gál P. Calcium-dependent conformational flexibility of a CUB domain controls activation of the complement serine protease C1r. Journal of Biological Chemistry. 2010;285:11863–9.
28. Kuznetsova SA, Mahoney DJ, Martin-Manso G, Ali T, Nentwich HA, Sipes JM, et al. TSG-6 binds via its CUB_C domain to the cell-binding domain of fibronectin and increases fibronectin matrix assembly. Matrix Biology. 2008;27:201–10.
29. Wisniewski HG, Hua JC, Poppers DM, Naime D, Vilcek J, Cronstein BN. TNF/IL-1-inducible protein TSG-6 potentiates plasmin inhibition by inter-alpha-inhibitor and exerts a strong anti-inflammatory effect in vivo. Journal of Immunology 1996;156:1609–15.
30. Maina V, Cotena A, Doni A, Nebuloni M, Pasqualini F, Milner CM, et al. Coregulation in human leukocytes of the long pentraxin PTX3 and TSG-6. Journal of Leukocyte Biology. 2009;86:123–32.
31. Bárdos T, Kamath RV, Mikecz K, Glant TT. Anti-inflammatory and chondroprotective effect of TSG-6 (tumor necrosis factor-alpha-stimulated gene-6) in murine models of experimental arthritis. American Journal of Pathology. 2001;159:1711–21.
32. Mindrescu C, Thorbecke GJ, Klein MJ, Vilcek J, Wisniewski HG. Amelioration of collagen-induced arthritis in DBA/1J mice by recombinant TSG-6, a tumor necrosis factor/interleukin-1-inducible protein. Arthritis & Rheumatology. 2000;43:2668–77.
33. Lesley J, Gál I, Mahoney DJ, Cordell MR, Rugg MS, Hyman R, et al. TSG-6 modulates the interaction between hyaluronan and cell surface CD44. J Biol Chem. 2004;279:25745–54.
34. Szántó S, Bárdos T, Gál I, Glant TT, Mikecz K. Enhanced neutrophil extravasation and rapid progression of proteoglycan-induced arthritis in TSG-6-knockout mice. Arthritis & Rheumatology. 2004;50:3012–22.

35. Lesley J, English NM, Gál I, Mikecz K, Day AJ, Hyman R. Hyaluronan binding properties of a CD44 chimera containing the link module Of TSG-6. Journal of Biological Chemistry 2002;277:26600–8. .
36. Hutás G BE, Gál I, Finnegan A, Glant TT, Mikecz K. CD44-specific antibody treatment and CD44 deficiency exert distinct effects on leukocyte recruitment in experimental arthritis. Blood. 2008;2008 December 15.:4999-5006.
37. Glant T, Cs-Szabó G, Nagase H, Jacobs J, K M. Progressive polyarthritis induced in BALB/c mice by aggrecan from normal and osteoarthritic human cartilage. Arthritis and Rheumatism. 1998;41:1007-18.
38. Glant T, Mikecz K, Arzoumanian A, Poole A. Proteoglycan-induced arthritis in BALB/c mice. Clinical features and histopathology. Arthritis and Rheumatism. 1987;30:201-12.
39. Rosenberg L. Chemical basis for the histological use of safranin-O in the study of articular cartilage. J Bone Joint Surg. 1971;53-A:69–82.
40. Westling J, Fosang A, Last K, Thompson V, Tomkinson K, Hebert T, et al. ADAMTS4 cleaves at the aggrecanase site (Glu373-Ala374) and secondarily at the matrix metalloproteinase site (Asn341-Phe342) in the aggrecaninterglobular domain. J Biol Chem. 2002;227:16059–66.
41. Nagase H, Kashiwagi M. Aggrecanases and cartilage matrix degradation. Arthritis Res Ther. 2003;5:94–103. .
42. Lahm A, Mrosek E, Spank H, Erggelet C, Kasch R, Esser J, et al. Changes in content and synthesis of collagen types and proteoglycans in osteoarthritis of the knee joint and comparison of quantitative analysis with Photoshop-based image analysis. Arch Orthop Trauma Surg. 2010;130:557–64.
43. Livak K, Schmittgen T. Analysis of relative gene expression data using real-time quantitative PCR and the 2(-Delta DeltaC(T)) method. Methods in Enzymology. 2001;25:402–8.
44. Glant TT, Kamath RV, Bárdos T, Gál I, Szántó S, Murad YM, et al. Cartilage-specific constitutive expression of TSG-6 protein (product of tumor necrosis factor alpha-stimulated gene 6) provides a chondroprotective, but not antiinflammatory, effect in antigen-induced arthritis. Arthritis Rheum. 2002;46:2207–18.
45. Köhler G, Milstein C. Continuous cultures of fused cells secreting antibody of predefined specificity. Nature. 1975;256:495–7.
46. Glant TT, Mikecz K, Poole AR. Monoclonal antibodies to different protein-related epitopes of human articular cartilage proteoglycans. Biochem J. 1986;234:31–41.
47. Zielen S, Bröker M, Strnad N, Schwenen L, Schön P, Gottwald G, et al. Simple determination of polysaccharide specific antibodies by means of chemically modified ELISA plates. J Immunol Methods. 1996;193:1–7.
48. Shi M, Dennis K, Peschon JJ, Chandrasekaran R, Mikecz K. Antibody-induced shedding of CD44 from adherent cells is linked to the assembly of the cytoskeleton. J Immunol. 2001;167:123–31.
49. Tiilikainen P, Pirttiniemi P, Kainulainen T, Pernu H, Raustia A. MMP-3 and -8 expression is found in the condylar surface of temporomandibular joints with internal derangement. J Oral Pathol Med. 2005;34:39–45.
50. Fernandes J, Martel-Pelletier J, Pelletier J. The role of cytokines in osteoarthritis pathophysiology
Biorheology. 2002;39:237–46.

51. Kobayashi M, Squires G, Mousa A, Tanzer M, Zukor D, Antoniou J, et al. Role of interleukin-1 and tumor necrosis factor alpha in matrix degradation of human osteoarthritic cartilage. Arthritis Rheum. 2005;52:128–35.
52. Hanyecz A, Berlo S, Szántó S, Broeren C, Mikecz K, Glant T. Achievement of a synergistic adjuvant effect on arthritis induction by activation of innate immunity and forcing the immune response toward the Th1 phenotype. Arthritis and Rheumatism. 2004;2004 May:1665-76.
53. Adarichev VA, Vermes C, Hanyecz A, Mikecz K, Bremer EG, Glant TT. Gene expression profiling in murine autoimmune arthritis during the initiation and progression of joint inflammation. Arthritis Research & Therapy. 2005;7:R196–R207.
54. Mahoney DJ, Mulloy B, Forster MJ, Blundell CD, Fries E, Milner CM, et al. Characterization of the interaction between tumor necrosis factor-stimulated gene-6 and heparin: implications for the inhibition of plasmin in extracellular matrix microenvironments. J Biol Chem. 2005;280:27044–55.
55. Higman VA, Blundell CD, Mahoney DJ, Redfield C, Noble ME, Day A. Plasticity of the TSG-6 HA-binding loop and mobility in the TSG-6-HA complex revealed by NMR and X-ray crystallography. Journal of Molecular Biology 2007;371:669–84.
56. Pejler G, Rönnberg E, Waern I, Wernersson S. Mast cell proteases: multifaceted regulators of inflammatory disease. Blood. 2010;115:4981–90.
57. Kolset SO, Prydz K, Pejler G. Intracellular proteoglycans. Biochem J. 2004;379:217–27.
58. Eggli P. S. GW. Cytochemical localization of hyaluronan in rat and human skin mast cell granules. J Invest Dermatol. 1993;100:121–5.
59. Kohda D. MCJ, Parkar A. A., Hatanaka H., Inagaki F. M., Campbell I. D., Day A. J. . Solution structure of the link module: a hyaluronan-binding domain involved in extracellular matrix stability and cell migration. Cell 1996;86:767–75.
60. Lee TH, Wisniewski HG, Vilcek J. A novel secretory tumor necrosis factor-inducible protein (TSG-6) is a member of the family of hyaluronate binding proteins, closely related to the adhesion receptor CD44. Journal of Cell Biology. 1992;116:545–57.
61. Wisniewski HG, Burgess WH, Oppenheim JD, Vilcek J. TSG-6, an arthritis-associated hyaluronan binding protein, forms a stable complex with the serum protein inter-alpha-inhibitor. Biochemistry. 1994;33:7423–9.
62. Wadhwa S, Embree M, Ameye L, Young M. Mice deficient in biglycan and fibromodulin as a model for temporomandibular joint osteoarthritis. cells, tissues, organs. 2005;181:136-43.
63. Hajati A, Alstergren P, Nasstrom K, Bratt J, Kopp S. Endogenous glutamate in association with inflammatory and hormonal factors modulates bone tissue resorption of the temporomandibular joint in patients with early rheumatoid arthritis. Journal of Oral and Maxillofacial Surgery. 2009;67:1895–903.
64. Alstergren P, Benavente C, Kopp S. Interleukin-1beta, interleukin-1 receptor antagonist, and interleukin-1 soluble receptor II in temporomandibular joint synovial fluid from patients with chronic polyarthritides. Journal of Oral and Maxillofacial Surgery 2003;61:1171–78.
65. Yoshida K, Takatsuka S, Hatada E, Nakamura H, Tanaka A, Ueki K, et al. Expression of matrix metalloproteinases and aggrecanase in the synovial fluids of patients with symptomatic temporomandibular disorders. Oral Surgery, Oral Medicine, Oral Pathology, Oral Radiology, and Endodontology 2006;102:22–7.
66. Martel-Pelletier J. Pathophysiology of osteoarthritis. Osteoarthritis and Cartilage. 1998;6:374–76.

67. Silbermann M LE. Age-related degenerative changes in the mouse mandibularjoint. Journal of Anatomy. 1979;129:507-20.
68. Glasson S, Askew R, Sheppard B, Carito B, Blanchet T, Ma H, et al. Deletion of active ADAMTS5 prevents cartilage degradation in a murine model of osteoarthritis. Nature. 2005;434:644-8.
69. Stanton H, Rogerson F, East C, Golub S, Lawlor K, Meeker C, et al. ADAMTS5 is the major aggrecanase in mouse cartilage in vivo and in vitro. Nature. 2005;434:648-52.
70. Wolfe G, MacNaul K, Buechel F, McDonnell J, Hoerrner L, Lark M, et al. Differential in vivo expression of collagenase messenger RNA in synovium and cartilage. Quantitative comparison with stromelysin messenger RNA levels in human rheumatoid arthritis and osteoarthritis patients and in two animal models of acute inflammatory arthritis. Arthritis and Rheumatism. 1993;36:1540-7.
71. Gack S, Vallon R, Schmidt J, Grigoriadis A, Tuckermann J, Schenkel J, et al. Expression of interstitial collagenase during skeletal development of the mouse is restricted to osteoblast-like cells and hypertrophic chondrocytes. Cell Growth and Differentiation. 1005;6:759-67.
72. Shlopov B, Lie W, Mainardi C, Cole A, Chubinskaya S, Hasty K. Osteoarthritic lesions: involvement of three different collagenases. Arthritis and Rheumatism. 1997;40:2065-74.
73. Gepstein A, Arbel G, Blumenfeld I, Peled M, Livne E. Association of metalloproteinases, tissue inhibitors of matrix metalloproteinases, and proteoglycans with development, aging, and osteoarthritis processes in mouse temporomandibular joint. Histochemistry And Cell Biology. 2003;120:23-32.
74. Gepstein A, Shapiro S, Arbel G, Lahat N, Livne E. Expression of matrix metalloproteinases in articular cartilage of temporomandibular and knee joints of mice during growth, maturation, and aging. Arthritis and Rheumatology. 2002 46:3240-50.
75. Blumenfeld I, Laufer D, Livne E. Effects of transforming growth factor-beta 1 and interleukin-1 alpha on matrix synthesis in osteoarthritic cartilage of the temporo-mandibular joint in aged mice. Mechanism of Aging and Development 1997;95:101-11.
76. Fu K, Ma X, Zhang Z, Pang X, Chen W. Interleukin-6 in synovial fluid and HLA-DR expression in synovium from patients with temporomandibular disorders. . Journal of Orofacial Pain. 1995;9:131–37.
77. Vernal R, Velasquez E, Gamonal J, Garcia-Sanz J, Silva A, Sanz M. Expression of proinflammatory cytokines in osteoarthritis of the temporomandibular joint. . Archives of Oral Biology. 2008;53:910–5.
78. Cohen S, Hurd E, Cush J, Schiff M, Weinblatt M, Moreland L, et al. Treatment of rheumatoid arthritis with anakinra, a recombinant human interleukin-1 receptor antagonist, in combination with methotrexate: results of a twenty-four-week, multicenter, randomized, double-blind, placebo-controlled trial. Arthritis Rheum. 2002;46:614–24.
79. Abramson S, Amin A. Blocking the effects of IL-1 in rheumatoid arthritis protects bone and cartilage. Rheumatology (Oxford). 2002;41:972–80.
80. Galli SJ, Grimbaldeston M, Tsai M. Immunomodulatory mast cells: negative, as well as positive, regulators of innate and acquired immunity. Nature Reviews Immunology. 2008;8:478–86.
81. McNeil HP, Adachi R, Stevens RL. Mast cell-restricted tryptases: structure and function in inflammation and pathogen defense. J Biol Chem. 2007;282:20785–9.
82. Crisp AJ, Chapman CM, Kirkham SE, Schiller AL, Krane SM. Articular mastocytosis in rheumatoid arthritis. Arthritis & Rheumatology. 1984;27:845–51.

83. Shin K, Gurish MF, Friend DS, Pemberton AD, Thornton EM, Miller HR, et al. Lymphocyte-independent connective tissue mast cells populate murine synovium. Arthritis Rheum 2006;54:2863–71.
84. Gruber BL, Marchese MJ, Suzuki K, Schwartz LB, Okada Y, Nagase H, et al. Synovial procollagenase activation by human mast cell tryptase dependence upon matrix metalloproteinase 3 activation. J Clin Invest 1989;84:1657–62.
85. Angyal A, Egelston C, Kobezda T, Olasz K, László A, Glant T, et al. Development of proteoglycan-induced arthritis depends on T cell-supported autoantibody production, but does not involve significant influx of T cells into the joints. Arthritis Research and Therapy. 2010;44.
86. McNeil HP, Shin K, Campbell IK, Wicks IP, Adachi R, Lee DM, et al. The mouse mast cell-restricted tetramer-forming tryptases mouse mast cell protease 6 and mouse mast cell protease 7 are critical mediators in inflammatory arthritis. Arthritis Rheum. 2008;58:2338–46.
87. Shin K, Nigrovic PA, Crish J, Boilard E, McNei lHP, Larabee KS, et al. Mast cells contribute to autoimmune inflammatory arthritis via their tryptase/heparin complexes. J Immunol. 2009;182:647–56.
88. Bjelle A, Norberg B, Sjögren G. The cytology of joint exudates in rheumatoid arthritis. Morphology and preparation techniques. . Scand J Rheumatol. 1982;11:124–8.
89. Getting SJ, Mahoney DJ, Cao T, Rugg MS, Fries E, Milner CM, et al. The link module from human TSG-6 inhibits neutrophil migration in a hyaluronan- and inter-alpha -inhibitor-independent manner. J Biol Chem. 2002;277:51068–76.
90. Mukhopadhyay D, Asari A, Rugg MS, Day AJ, Fülöp C. Specificity of the tumor necrosis factor-induced protein 6-mediated heavy chain transfer from inter-alpha-trypsin inhibitor to hyaluronan: implications for the assembly of the cumulus extracellular matrix. Journal of Biological Chemistry. 2004;279:11119–28.
91. Sanggaard KW, Hansen L, Scavenius C, Wisniewski HG, Kristensen T, Thøgersen IB, et al. Evolutionary conservation of heavy chain protein transfer between glycosaminoglycans. Biochimica et Biophysica 2010;1804:1011–9. .
92. Itoh H, Ide H, Ishikawa N, Nawa Y. Mast cell protease inhibitor, trypstatin, is a fragment of inter-alpha-trypsin inhibitor light chain. Journal of Biology 1994;269:3818–22.
93. Ide H, Itoh H, Yoshida E, Kobayashi T, Tomita M, Maruyama H, et al. Immunohistochemical demonstration of inter-alpha-trypsin inhibitor light chain (bikunin) in human mast cells. . Cell and Tissue Research. 1999;297:149–54.

Acknowledgements

I would like to express my sincere gratitude to my supervisor Professor Zoltan Szekanecz, for his patience, motivation, his guidance and for the continuous support of my Ph.D study. My sincere thanks also goes to professor Tibor G Glant and Professor Katalin Mikesz who provided me an opportunity to join their team, supported and guided me and gave access to their laboratory and research facilities. Without they precious support it would not be possible to conduct this research.

Last but not the least, I would like to thank to my mother-in law Dr Margit Fuxaiture and My late father-in-law Professor Gyorgy Szekely, my mother and to my brother and sister for supporting me spiritually throughout writing this thesis and my life in general.

At the end I would like to express my special appreciation and thanks to my beloved husband Dr Tamas Kobezda for all his help and support, words cannot express how grateful I am.

Publications

UNIVERSITY AND NATIONAL LIBRAY
UNIVERSITY OF DEBRECEN
H-4002 Egyetem tér 1, Debrecen
Phone: +3652/410-443, email: publikaciok@lib.unideb.hu

Registry number: DEENK//2017.PL
Subject: PhD Publikációs Lista

Candidate: Sheida Ghassemi-Nejad
Neptun ID: OLPFDS
Doctoral School: Doctoral School of Clinical Medicine

List of publications related to the dissertation

1. **Ghassemi-Nejad, S.**, Kobezda, T., Tar, I., Szekanecz, Z.: Development of temporomandibular joint arthritis: the use of animal models.
   Joint Bone Spine. 84 (2), 145-151, 2017.
   DOI: http://dx.doi.org/10.1016/j.jbspin.2016.05.016
   IF: 3.329 (2016)

2. **Ghassemi-Nejad, S.**, Kobezda, T., Rauch, T. A., Matesz, K., Glant, T. T., Mikecz, K.: Osteoarthritis-like damage of cartilage in the temporomandibular joints in mice with autoimmune inflammatory arthritis.
   Osteoarthritis Cartilage. 19 (4), 458-465, 2011.
   DOI: http://dx.doi.org/10.1016/j.joca.2011.01.012
   IF: 3.904

3. Nagyeri, G., Radács, M., **Ghassemi-Nejad, S.**, Tryniszewska, B., Olasz, K., Hutas, G., Győrfy, Z., Hascall, V. C., Glant, T. T., Mikecz, K.: TSG-6 Protein, a Negative Regulator of Inflammatory Arthritis, Forms a Ternary Complex with Murine Mast Cell Tryptases and Heparin.
   J. Biol. Chem. 286 (26), 23559-23569, 2011.
   DOI: http://dx.doi.org/10.1074/jbc.M111.222026
   IF: 4.773

UNIVERSITY of DEBRECEN

UNIVERSITY AND NATIONAL LIBRAY
UNIVERSITY OF DEBRECEN
H-4002 Egyetem tér 1, Debrecen
Phone: +3652/410-443, email: publikaciok@lib.unideb.hu

List of other publications

4. Kobezda, T., **Ghassemi-Nejad, S.**, Mikecz, K., Glant, T. T., Szekanecz, Z.: Of mice and men: how animal models advance our understanding of T-cell function in RA.
   Nat. Rev. Rheumatol. 10 (3), 160-170, 2014.
   DOI: http://dx.doi.org/10.1038/nrrheum.2013.205
   IF: 9.845

5. Kobezda, T., **Ghassemi-Nejad, S.**, Glant, T. T., Mikecz, K.: In vivo two-photon imaging of T cell motility in joint-draining lymph nodes in a mouse model of rheumatoid arthritis.
   Cell. Immunol. 278 (1-2), 158-165, 2012.
   DOI: http://dx.doi.org/10.1016/j.cellimm.2012.08.003
   IF: 1.743

6. Nesterovitch, A. B., Szántó, S., Gonda, A., Bárdos, T., Kis-Tóth, K., Adarichev, V. A., Olasz, K., **Ghassemi-Nejad, S.**, Hoffman, M. D., Tharp, M. D., Mikecz, K., Glant, T. T.: Spontaneous insertion of a B2 element in the ptpn6 gene drives a systemic autoinflammatory disease in mice resembling neutrophilic dermatosis in humans.
   Am. J. Pathol. 178 (4), 1701-1714, 2011.
   DOI: http://dx.doi.org/10.1016/j.ajpath.2010.12.053
   IF: 4.89

Total IF of journals (all publications): 28,484
Total IF of journals (publications related to the dissertation): 12,006

The Candidate's publication data submitted to the iDEa Tudóstér have been validated by DEENK on the basis of Web of Science, Scopus and Journal Citation Report (Impact Factor) databases.

17 November, 2017

Presentations

- Temporomandibular joint involvement in mice with proteoglycan induced arthritis.
  Sheida Ghassemi-Nejad, Tamas Kobezda, Tibor T. Glant and Katalin Mikecz.
  Midwest Connective Tissue Workshop, Chicago, 2010

- In vivo imaging of T cell motility in the joint draining lymph nodes of genetically unmanipulated mice in a model of rheumatoid arthritis.
  Tamas Kobezda, **Sheida Ghassemi-Nejad**, Colt Egelston, Tibor T. Glant and Katalin Mikecz.
  American College of Rheumatology Annual Scientific Meeting, Chicago, 2011

- Dancing with the stars: In vivo imaging of immune cells in the joints and joint draining lymph nodes of mice with proteoglycan induced arthritis
  Tamas Kobezda, **Sheida Ghassemi-Nejad**, Colt Egelston, Tibor T. Glant and KatalinMikecz
  Midwest Connective Tissue Workshop, Chicago, 2010

Posters

- Temporomandibular joint involvement in mice with proteoglycan induced arthritis.
  Sheida Ghassemi-Nejad, Tamas Kobezda, Tibor T. Glant and Katalin Mikecz.
  Midwest Connective Tissue Workshop, Chicago, USA, 2010
- In vivo amaging of T cell motility in the joint draining lymph nodes of genetically unmanipulated mice in a model of rheumatoid arthritis.
  Tamas Kobezda, **Sheida Ghassemi-Nejad**, Colt Egelston, Tibor T. Glant and Katalin Mikecz.
  American College of Rheumatology Annual Scientific Meeting, Chicago, USA, 2011

- Dancing with the stars: In vivo imaging of immune cells in the joints and joint draining lymph nodes of mice with proteoglycan induced arthritis
  Tamas Kobezda, **Sheida Ghassemi-Nejad**, Colt Egelston, Tibor T. Glant and Katalin Mikecz
  Midwest Connective Tissue Workshop, Chicago,USA, 2010

- Characterization of the trafficking and motility of T cells in the joints and joint-draining lymph nodes in an autoimmune murine model of rheumatoid arthritis
  Tamás Kobezda **, Sheida Ghassemi Nejad,** Tibor T. Glant, Katalin Mikecz and Zoltan Szekanecz
  School of surgery conference, Doncaster, UK 2014
- Development of osteoarthritis: the use of animal Model
  Tamás Kobezda**, Sheida Ghassemi Nejad,** and Zoltan Szekanecz
  EMSORD, Leicester, UK, 2016